STUDY OF SPACE-TIME EVOLUTION OF FLUX IN A LONG-LIFE TRAVELING WAVE REACTOR

BY

RIJAN PRASAD SHRESTHA

THESIS

Submitted in partial fulfillment of the requirements
for the degree of Master of Science in Nuclear, Plasma and Radiological Engineering
in the Graduate College of the
University of Illinois at Urbana-Champaign, 2012

Urbana, Illinois

Master's Committee:

Professor Rizwan Uddin, Chair
Assistant Professor Tomasz Kozlowski

Abstract

Simulations using MCNPX have been carried out to analyze the space and time evolution of flux in a Traveling Wave Reactor under constant thermal power condition. For the analyses of flux shape, a 3-D box-shaped model of the reactor is developed. The reactor core is divided into two primary regions: the smaller, enriched region with fissile material; and the larger non-enriched region with fertile material. This enrichment strategy is aimed to allow breed-and-burn in the core. The core, on the outside, is surrounded by reflector of uniform thickness. To facilitate the study of flux profile, the two primary regions in the core are further divided into finer thin slab-like regions called cells. Results presented in this thesis show the propagation of flux profile from the enriched region to the non-enriched region at a near constant speed. This shift in the flux profile is due to the continuous breeding of fissile material and its immediate burning. Analyses of local power density (power fraction) at three specified locations in the core as a function of time are presented. Space and time evolution of the overall core burn-up and localized burn-up are presented and discussed. A history of inventory, according to mass, is reported for selected nuclides. Simplified thermal-hydraulics analysis is carried out to estimate the core-averaged velocity and mass flow rate of sodium coolant through the core. Spatially varying velocity profile and corresponding coolant flow rate based on flux profile (local power density) at any given time is also reported.

Acknowledgement

I would like to express to my sincere gratitude towards my advisor Professor Rizwan-uddin for his valuable support throughout this project. Thanks for guiding me through this research project and providing many helpful insights. This work would not have been completed without his time, patience and understanding. I would also like to thank Professor Tomasz Kozlowski for serving as the reader for this thesis.

I would like to thank my dear friends Santosh Koirala, Abhiskeh Jaiswal and Wu Hsingtzu for their genuine friendship and encouragement. Special thanks to Rabie Abu Saleem, you were there willing to help me any day, any time. I would also like to acknowledge all the faculty and staff of NPRE for their continuous help and wisdom.

Finally, I would also like to thank the two most important people in my life, my parents, for their continuous support and encouragement; I would have been nowhere close to this without their love and patience.

Rijan P Shrestha

Table of Contents

List of Tables

List of Figures

Nomenclature

ANL	Argonne National Laboratory
BOL	beginning of life
CANDLE	Constant Axial shape of Neutron flux, Densities and power shape during Life of Energy producing reactor
CR	conversion ratio
EBR	Experimental Breeder Reactor
ENDF/B	Evaluated Nuclear Data File B-version
EOL	end of life
k_{eff}	k-effective
LWR	Light Water Reactor
NU	natural uranium
SMFR	Small Modular Fast Reactor
TH	thermal-hydraulicss
TWR	Traveling Wave Reactor
η	neutron yield per neutron absorbed
c	specific heat capacity, MJ/K-m^3

Chapter 1

Introduction

Coal, oil and natural gas had been the main sources of world energy before the advent of nuclear power. With the discovery of nuclear fission in 1930s, it was hoped that nuclear power could someday supplement world's growing energy demands. By late 1940s, the physics behind the fission of ^{233}U, ^{235}U and ^{239}Pu were completely understood. These isotopes that undergo fission to release energy are called fissile isotopes. Electricity was first generated using controlled nuclear fission on December 20, 1951 at EBR-I in Arco, Idaho. In 1953, US President Dwight Eisenhower endorsed peaceful use of nuclear energy in his "Atoms for Peace" speech at the United Nations. Obninsk Nuclear Power Plant in Russia became the world's first nuclear power plant to generate electricity for a power grid in 1954.

Nuclides like ^{238}U and ^{232}Th capture neutrons and decay to fissile isotopes ^{239}Pu and ^{233}U, respectively. Isotopes that are converted to fissile isotopes by neutron capture and subsequent decay are called fertile isotopes. It was found that fertile isotopes alone were not sufficient to sustain a nuclear chain reaction; fissile isotopes were needed. Since fissile isotopes are present in a very limited quantity in natural state (0.7% ^{235}U in natural uranium), conversion of fertile isotopes to fissile isotopes by neutron capture was proposed as a method to produce fissile isotopes, and hence sustain a chain reaction using fertile materials. This was termed breeding.

Neutrons with energy ranging from just above 0 eV to around 1 MeV are good for breeding. Neutrons with energy less than 0.1 eV are called thermal neutrons and those with energy higher than 0.1 MeV are called fast neutrons. It was observed that breeding was more efficient with fast neutrons than thermal neutrons. Most reactors operating today rely primarily on thermal neutrons for fission. Hence, in these reactors, such as the Light Water Reactors (LWRs), the neutrons are

made to slow down and thermalize by a moderator. These are called thermal reactors. In contrast, nuclear reactors that operate primarily using fast neutrons (without neutron moderation) are called fast spectrum reactors or simply fast reactors. The breeding of fissile materials from fertile isotopes make fast reactors very effective in utilizing uranium resources compared to thermal reactors such as the Light Water Reactors (LWRs), i.e. more energy could be extracted from fast reactors than LWRs per unit mass of fuel. Traveling Wave Reactor (TWR) is a specific variant of fast breeder reactor that primarily has two or more zones of varying enrichment along the axial direction of the core and utilizes breeding along the axial direction for in-situ production of fissile isotopes.

1.1 Theory

Fertile isotopes ^{238}U and ^{232}Th are respectively converted to fissile isotopes ^{239}Pu and ^{233}U by neutron capture (n, γ) reactions. A ^{238}U atom captures a neutron and is converted to ^{239}U with an emission of a gamma ray. The ^{239}U atom undergoes beta decay with a half-life of 23.5 minutes to ^{239}Np which further undergoes beta decay with a half-life of 2.35 days to ^{239}Pu, which is fissile. This isotope of ^{239}Pu can either undergo fission directly or can be converted further to ^{240}Pu by another neutron capture. The ^{238}U-^{239}Pu cycle is shown in Figure 1.1.

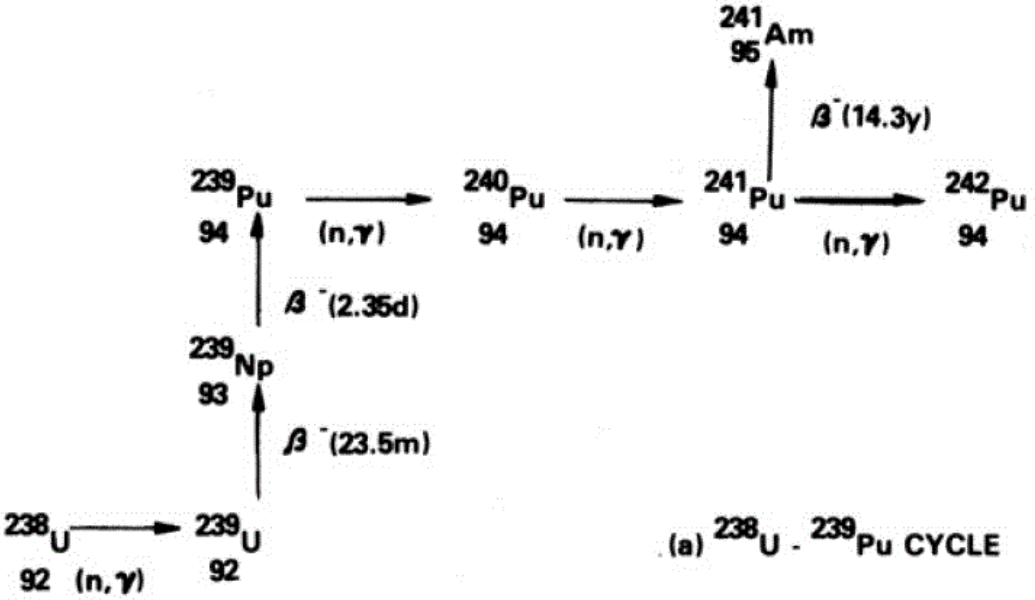

Figure 1.1: ^{238}U-^{239}Pu conversion chain [1]

Figure 1.2 shows the ^{232}Th-^{233}U cycle which could be used as an alternative cycle for breeding of fissile materials in a fast reactor.

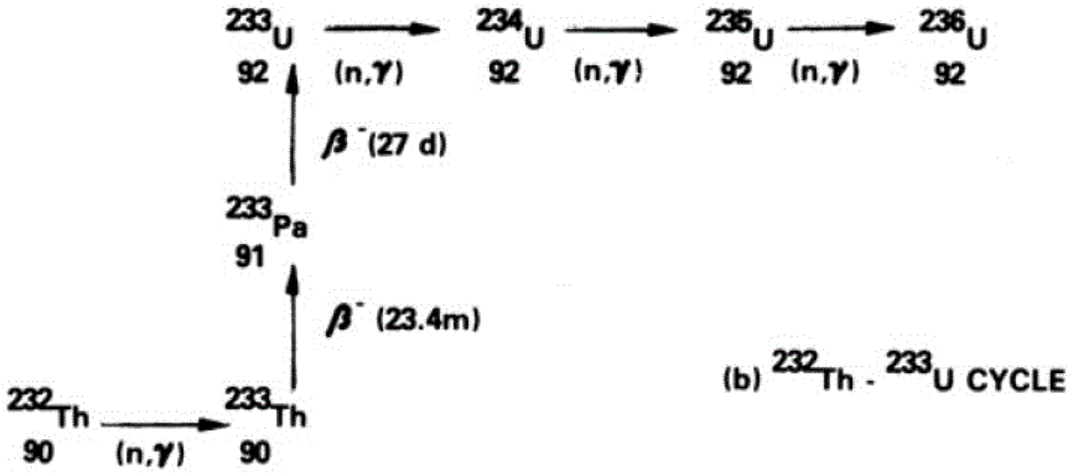

Figure 1.2: ^{232}Th-^{233}U conversion chain [1]

The TWR in this study is to operate primarily under ^{238}U-^{239}Pu breeding cycle. It follows breed-and-burn principle, i.e. breeding of fissile isotope occurs first which is then followed by its fission. This continuous breeding and burning moves along an axial direction in the core defined by fuel loading and core geometry (details are presented in Chapter 3). The name Traveling Wave Reactor is derived from this propagation of breed-and-burn waves along an axial direction in the core. A once-through fuel cycle is implemented, i.e. there is no reshuffling of fuel elements during reactor operation. Owing to the hard spectrum in fast reactors, of which TWR is a specific variant, the fuel does not need a rigorous reprocessing before long term storage.

Cross sections of fissile materials are generally greater for neutron in the thermal energy range than in fast energy range. Figure 1.3 shows principal cross sections of ^{239}Pu plotted using ENDF/B-VII library [2]. Figure is taken from Ref. [3]. It can be seen from Figure 1.3 that the cross sections are orders of magnitude greater in the thermal range than in the fast energy range. This suggests a better neutron economy in a thermal reactor. However, fast reactors are more desirable owing to the better fuel efficiency, the prospect of burning most minor actinides, and a once-through fuel cycle with no reprocessing. Moreover, the relatively inefficient neutron economy in a fast reactor is balanced by the higher reproduction factor (η) which is a measure of net neutron yield per neutron absorbed in the fuel. Reproduction factor for different isotopes are shown in Figure 1.4. Clearly, η for ^{239}Pu and ^{233}U are much larger in fast energy range than in the thermal range.

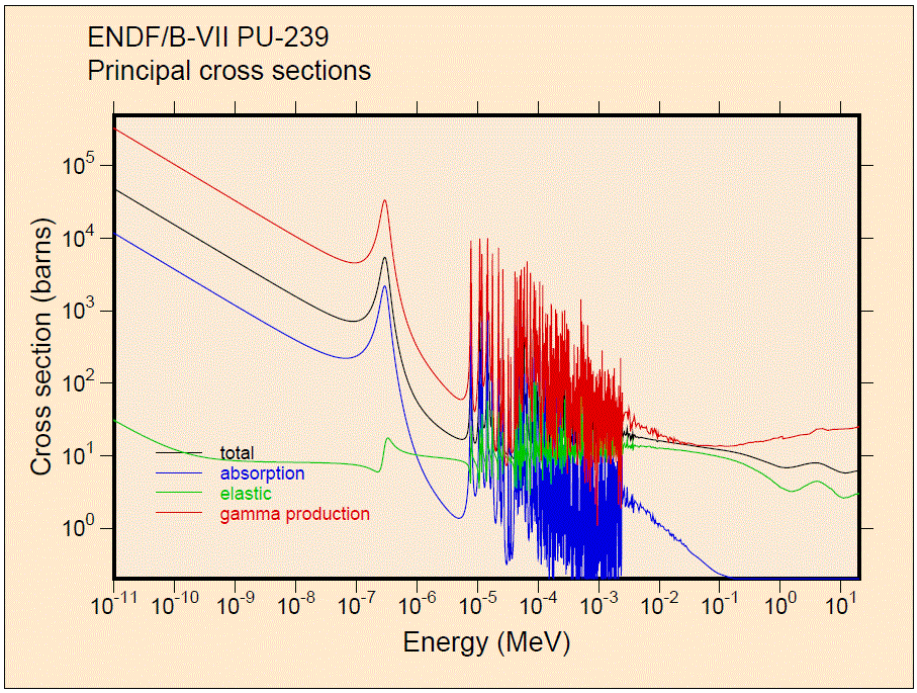

Figure 1.3: Energy-dependent cross section of ^{239}Pu [3]

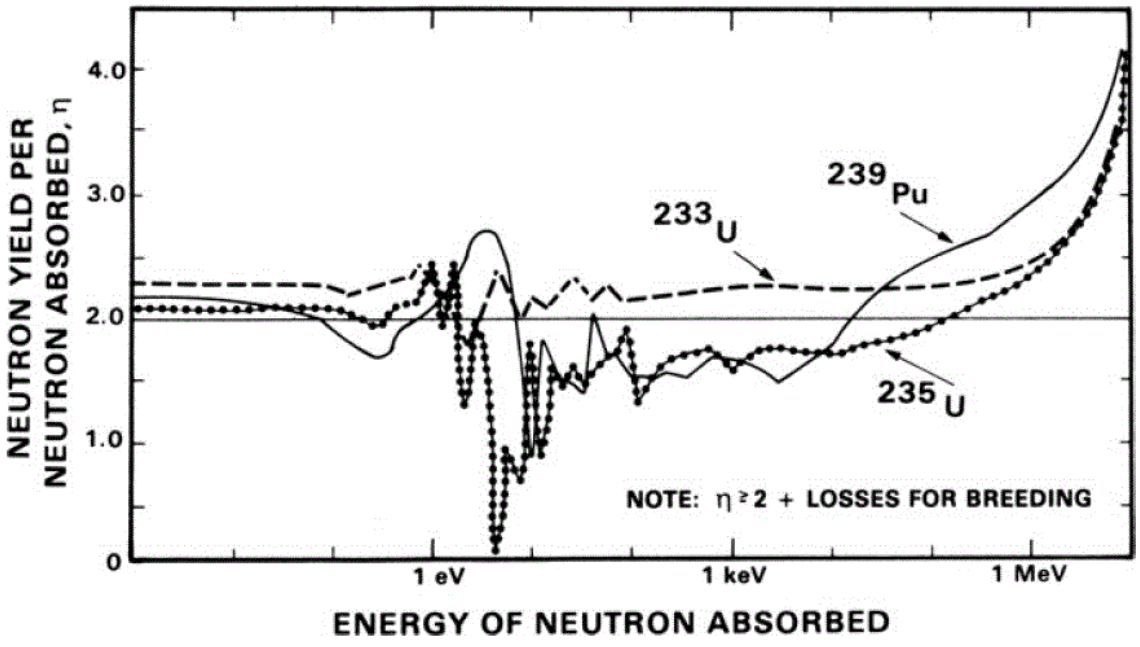

Figure 1.4: Neutron yield per neutron absorbed vs. incident neutron energy [1]

Conversion ratio (CR) is a parameter that gives the ratio of fissile material produced to fissile material destroyed. For a safe operation, it is desirable that a TWR have a CR of close to 1. This will also ensure criticality over the core lifetime. However, the core should have excess reactivity at Beginning of Life (BOL). Xenon poisoning immediately after start-up should be balanced by excess reactivity at BOL. This will allow the core to operate in a critical configuration at latter stages (details are presented in section 4.3).

1.2 Objectives

Safe and sustainable production of electricity from nuclear fission along with the desire to minimize nuclear waste has been a long-standing focus in the nuclear industry. Owing to the catastrophic disasters at Chernobyl and Three Mile Island, special consideration must be given to safety while designing future nuclear plants. In-built mechanisms to automatically prevent uncontrolled chain reaction must be present in the reactor. Limited availability of fissile isotopes in nature necessitates use of breeding for in-situ production of fissile materials. Moreover, a long reactor core lifetime and operation under once-through fuel cycle is desirable for economic and non-proliferation reasons.

The objective of this study can be broadly categorized into two parts. The first objective is to design a TWR core fulfilling aforementioned criteria. The second objective, which is the primary motivation of this study, is to present analyses of space-time evolution of flux shape, associated burn-ups and a history inventory of selected actinides in the core over its lifetime.

TerraPower Inc. is also conducting active research on designing a life-size Traveling Wave Reactor [4].

1.3 Thesis Organization

A brief outline of the structure of this thesis is presented in this section. Chapter 2 presents a discussion about previously recommended ideas and suggestions on TWR and closely related concepts. Chapter 3 presents an overview of the proposed TWR design. Discussions of results related to evolution of flux shape, associated burn-ups and actinide inventories are presented in Chapter 4. Chapter 5 presents discussions about thermal-hydraulics (TH) analyses in the core and recommends an appropriate TH engineering design. Finally, Chapter 6 presents a summary of the main ideas in this thesis and suggests relevant future work for potential improvement.

Chapter 2

Literature Survey

Future nuclear reactor technology aims at achieving longer core life, higher burn-up and higher uranium utilization in a proliferation resistant fuel cycle. Some relevant studies conducted in the past to achieve these objectives are reported in this chapter. The reported designs are fast spectrum systems that operate with or without fuel reshuffling. Burn-ups as high as 400 GW-d/MTU have been reported for some designs. Other proposed designs aim at achieving an extremely long core life; as long as 100 years. Models characterized by uranium utilization around 30% have also been proposed. (For LWRs, less than 1% uranium utilization is observed.)

2.1 Analytical studies

Breed-and-burn mode was first suggested in 1958 by Russian physicist Feinberg [5]. He proposed a self-regulating fast reactor without any control mechanism. Criticality in the core was to be maintained over long time by a combination of appropriate fissile and fertile materials in an appropriate geometrical configuration. More recently, another Russian physicist, L. Feoktistov, proposed a Traveling Wave Reactor which is to operate under the same principles of breed-and-burn using the uranium-plutonium fuel cycle [6],

$$^{238}\mathrm{U}\ (\mathrm{n}, \gamma) \rightarrow {}^{239}\mathrm{U} \rightarrow {}^{239}\mathrm{Np} \rightarrow {}^{239}\mathrm{Pu}\ (\mathrm{n}, \text{fission}). \qquad 2.1.1$$

Recently, further analyses are reported by Rusov and colleagues on Feoktistov's self-regulating wave on theoretical understanding for existence of nuclear burning wave in neutron-multiplying media. They found that the condition for soliton-like wave is determined primarily by two parameters, viz. the relationship between equilibrium and critical concentrations of fissionable isotopes and Wigner quantum statistics [7].

Chen and Maschek showed the existence of a permanent plane solitary wave in a fertile medium using one-group diffusion equation coupled with burn-up equations. Furthermore, they found that the solitary wave also had a constant reactivity [8].

2.2 Numerical studies

Teller, Ishiwaka and Wood designed a breed-and-burn model of a reactor using Monte-Carlo based TART95 code. TART95 is a general-purpose neutron and gamma-ray three-dimensional transport and reaction-modeling code for neutronics. They claimed that the automation of the reactor would mean that the least-trained operators may be in charge without posing any danger to reactor operation [9]. They found that a cylinder of less than one meter diameter with natural uranium or thorium metal surrounded by a reflector may stably propagate nuclear waves for arbitrary distances. This result provides a strong boost to the feasibility of a reactor that operates with an extremely long core life. Furthermore, they reported a 70% burn-up in a core initially composed of ^{232}Th. They concluded that it is feasible to operate a nuclear reactor with a pure breed-and-burn propagation wave and maintain the steady-state conditions for an indefinite period.

Sekimoto and Miyashita proposed CANDLE (Constant Axial shape of Neuron flux, nuclide densities and power shape During Life of Energy production) burn-up strategy where overall neutron flux shape and power density distributions remain nearly the same over time but move along the axial position [10]. Similar to the model proposed by Teller it operates on breed-and-burn principles which are figuratively explained in Figure 2.1.

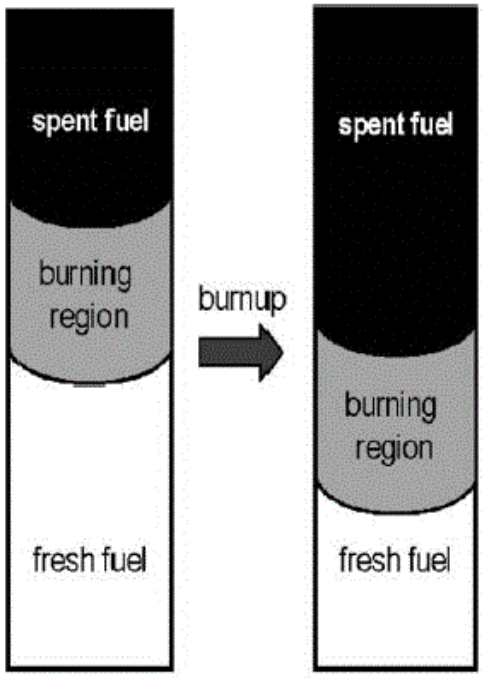

Figure 2.1: CANDLE burn-up strategy [11]

Sekimoto and Miyashita used the SRAC code system with JENDL 3.2 nuclear data library. The core composed of lead-bismuth coolant, and nitride fuel was found to yield a burn-up of 396 GWd/MTU and a steady wave propagation speed of 3.1 cm/year [11]. The axial movement of power density (or equivalently flux shape) is shown in Figure 2.2. Ideally, the model proposed by Sekimoto and Miyashita could maintain criticality for an indefinite time.

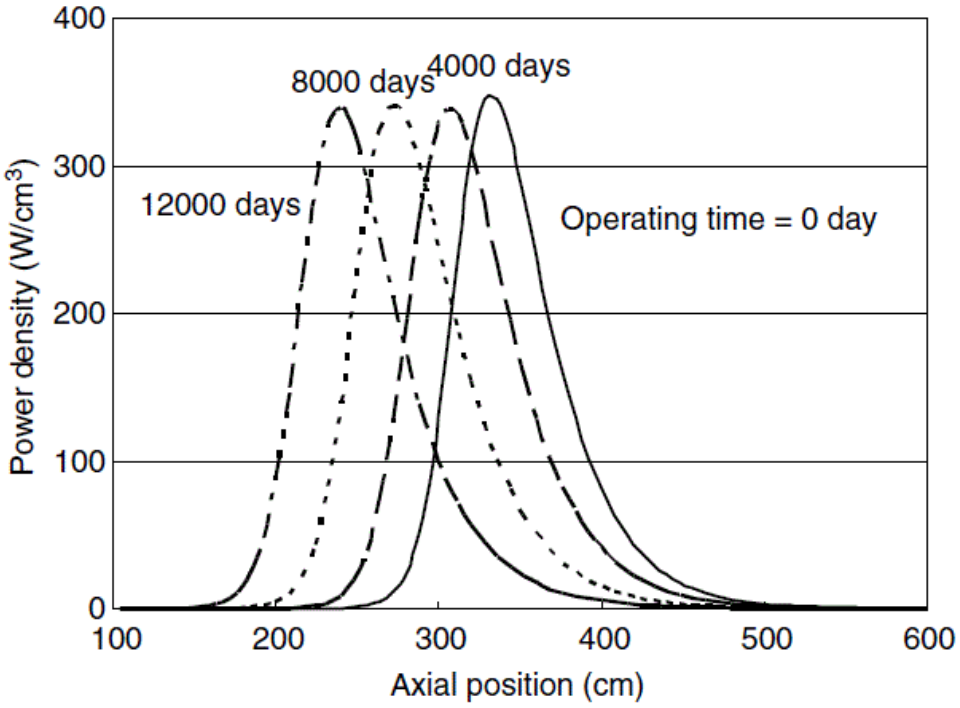

Figure 2.2: Power density distribution vs. axial position [11]

Fomin et al. used numerical modeling with effective multi-group diffusion equation and burn-up equations to demonstrate self-sustained regime of nuclear burning wave in a critical fast reactor with mixed Th-U fuel [12]. Result of space-time evolution of neutron flux is shown in Figure 2.3. Assurance of safety is shown by the stability of nuclear burning wave regime against neutron flux distortions in the reactor. It was demonstrated that a core life of 60 years for a cylindrical reactor of length 5 m could be achieved if the core was composed of ^{235}U and ^{239}Pu in the fissile region and ^{238}U and ^{232}Th in the breeding region. 50% burn-up was reported for this core. The velocity of the Nuclear Burning Wave (NBW) was reported to be 6 cm/year. They showed that the increase in radius of the cylinder led to a rapid increase of neutron flux in the system and, simultaneously, of the NBW speed. They also showed that a decrease in radius below a cut-off value could not sustain NBW.

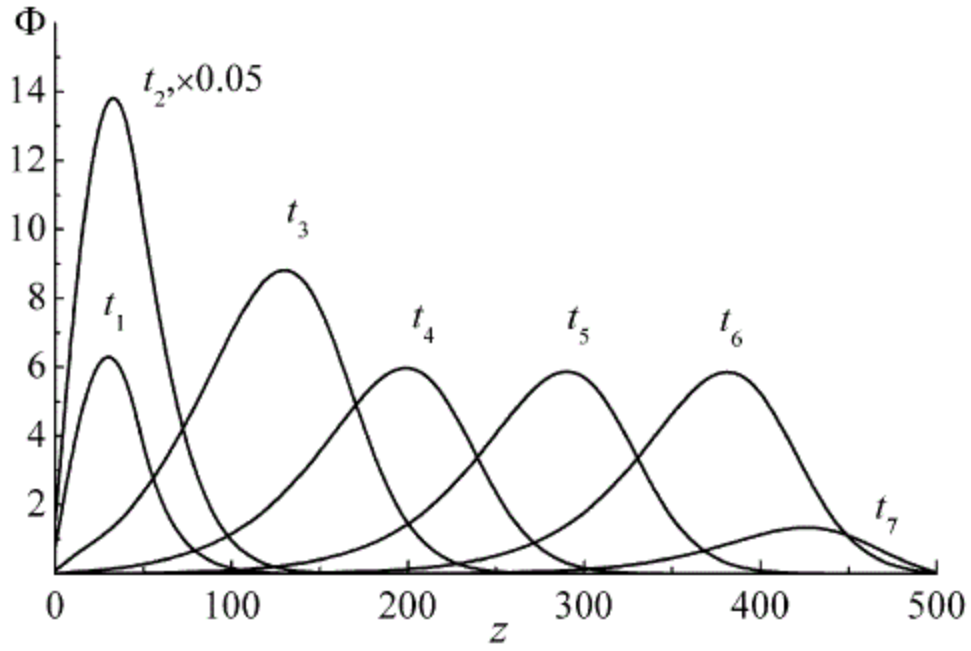

Figure 2.3: Un-normalized scalar neutron flux vs. axial position ($t_1 < t_2 < t_3 < t_4 < t_5 < t_6 < t_7$) [12]

The feasibility of propagation of a breed-and-burn wave in a fast reactor with an appropriate breeding region and an appropriate geometry has been established following preceding discussions. Most studies conducted in the past have analyzed breed-and-burn waves either with analytical techniques or using deterministic methods for simple one-dimensional cases. Detailed analyses for a 3-D case with continuous energy formulation using Monte Carlo methods are difficult to find in literature. This study uses stochastic Monte-Carlo MCNPX code to analyze a 3-D model of the TWR reactor with prescribed fissile and fertile (breeding) regions and provides results for space-time evolution of the flux shape.

Chapter 3

Core Design and Composition

Details for the design of reactor core are presented in this chapter. Studies conducted in the past recommend the use of elongated cores with zonal enrichment along the main axis to allow for breeding and burning which, in turn, facilitates a long core life. This is taken into consideration while designing the reactor core. Furthermore, enrichment strategies are discussed that keep the reactor close to critical throughout its lifetime. Following some preliminary calculations, a trial and error approach is followed to develop an appropriate configuration. Cladding and structural materials are chosen from recommendations put forth by Argonne National Laboratory's Small Modular Fast Reactor (ANL SMFR) Design Description report [13]. Unlike thermal reactors that require elaborate cell and assembly level homogenization before core physics can be analyzed, fast reactors could be modeled accurately using simple material homogenization techniques [14]. Homogenization of the core material is presented in this chapter based on volume fractions of associated core components. Finally, power level is specified as the flux normalization parameter and the time for which core physics is to be simulated is also specified.

3.1 Core geometry

A box-shaped 3-D homogeneous core is modeled using MCNPX v27c [15]. The choice of using a rectangular core (over a right circular cylinder) is arbitrary since the primary motivation of this study is to analyze the development of flux profile over the core life. However, a right circular cylinder is more efficient in minimizing fast leakage than a rectangular core and is better suited for a commercial design. A schematic diagram of the core is presented in Figure 3.1. The dimensions of the core are listed in Table 3.1.

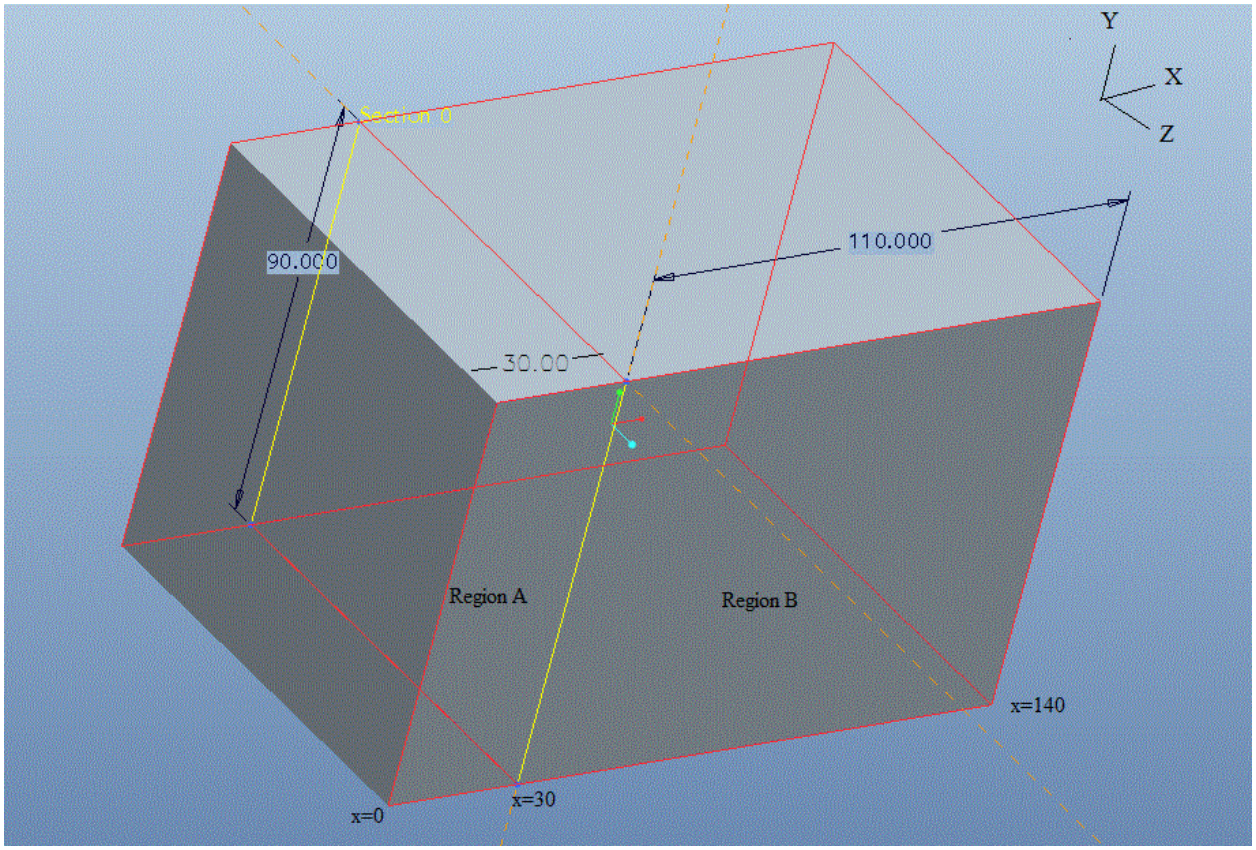

Figure 3.1: Schematic diagram of TWR core

X (cm)	Length (Axial)	140
Y (cm)	Width	90
Z (cm)	Height	90

Table 3.1: Core dimensions

The TWR core is divided into two regions of enrichment viz. region A ($0 < X < 30$ cm) and region B ($30 < X < 140$ cm). Furthermore, it is divided into smaller regions by planes parallel to the Y-Z plane in Figure 3.1. These planes are 2 cm apart. The model consists of 69 such parallel planes, thus dividing the core into 70 smaller slab-regions stacked along the positive X-axis, henceforth referred to as cells. Hence there are 15 cells in region A and 55 cells in region B.

Each cell has a volume of 16200 cm^3. Fuel, coolant, cladding and structural materials are loaded in individual cells as described in the following sections. Moreover, the TWR core is surrounded on all sides by a reflector, composed of HT9 and sodium, with a uniform thickness of 10 cm. HT9 is a low-swelling stainless steel, i.e. a ferritic alloy composed of 0.5 wt% Ni, 12 wt% Cr, 0.2 wt% Mn, 1 wt% Mo, 0.25 wt% Si, 0.5 Wt% W, 0.5 wt% V, and 0.2 wt% C, with the balance Fe [16].

Table 3.2 shows the volume and weight fractions of core composition in each cell. Core dimensions along with volumetric and weight fractions of fuel, coolant and structural materials reported here are the end results of a long and tedious iteration process aimed at satisfying the requirement of a long core life.

Composition of each cell	Volume fractions	Mass fractions
Fuel	0.85	0.956
Coolant	0.07	0.005
Structural material and cladding	0.08	0.039

Table 3.2: Volume and mass fractions of core composition in each cell

3.2 Metallic fuel

Metallic fuel is chosen following the recommendation from ANL SMFR report [13]. A higher peak burn-up of 12% was reported for metallic fuel compared to 9% for oxide fuel. Metal fuels are denser than oxide fuels, allowing for a higher specific power [13]. In addition to that, lack of oxygen makes the neutron spectrum harder, which is desirable. The fuel consists of 10% Zr and 90% U by weight. U-10 wt. % Zr is hence used as fuel in the model. The core is designed with fuel occupying 85% of each cell volume, or equivalently 85% of core volume. Owing to the relatively small size of the reactor core, a higher fuel volume fraction is needed to maintain criticality and to ensure a long core life. However, this might put an increased stress on thermal-

hydraulics requirements in the core. Analysis on core thermal-hydraulics is presented in Chapter 5.

3.2.1 Fuel enrichment by region

A parametric study was performed to ensure criticality of the core throughout its life. First, the enrichment region was defined. For example, either the first 10 cells (from the left) or the first 15 cells (in Figure 3.1) could be designated as cells containing enriched fuel while the rest could be designated as cells containing fuel fabricated with natural uranium (NU). Second, the enrichment level was specified. For example, the enriched cells could contain fuel enriched to either 25% in ^{235}U or 30% in ^{235}U. Simulations were carried out with various combinations of enrichment region and enrichment levels. If the reactor core went sub-critical after startup and stayed sub-critical for extended period without automatically returning to criticality during a simulation, that combination of enrichment region and enrichment level was rejected and a new set of design parameters was chosen for the next simulation. This study was conducted with the set of parameters that kept the TWR core close to critical ($k_{eff} \sim 1$) for a core life of nearly 40 years.

In the final analysis, cells in region A were enriched to 33% in ^{235}U and those in region B contained natural uranium. Hence region A ($0 < X < 30$ cm) is also referred to as enriched region and region B ($30 < X < 140$ cm) as non-enriched region.

3.3 Cladding and structural material

HT9 alloy was chosen as the material for cladding and structural support following recommendations from ANL SMFR design report [13]. In fast reactors, cladding and structural material should be corrosion resistant owing to irradiation by high fast flux ($\sim 10^{15}/cm^2$-sec) in the core. HT9 has also proven to be highly corrosion resistant in sodium [17]. For the simulation,

the combined volume fraction for cladding and structural material in the core was 8%. The low volume fraction for cladding and structural material was chosen to increase the fuel volume fraction and hence minimize the core size. Additionally, this also helped in reducing the CPU time needed for the large number of simulations and burn-up calculations necessary to test the design. Note that the core size of a commercial reactor is expected to be much larger than one used here. For example, the average Pressurized Water Reactor core has a radius of about 180 cm and an active fuel length of about 400 cm. The cylindrical TWR core proposed by Fomin et al. has a radius of 220 cm and an axial height of 500 cm [12]. By allowing enrichment greater than 20% and reducing the volume fraction of coolant and structural materials, a compact core can be designed, making a Monte-Carlo based criticality and burn-up calculations computationally affordable.

3.4 Coolant

Liquid sodium is used as the coolant in the core due to its favorable thermo-physical properties over other coolants for fast reactors. Liquid metals, in general, have high thermal conductivity, indifference to radiation and useful temperature range at low pressure [1]. Table 3.3 compares thermo-physical properties for some proposed fast reactor coolants.

Though the use of sodium as a coolant risks the possibility of solidification at room temperature, it should however be noted that sodium in the coolant pool is maintained at a temperature well above its melting point by reactor thermal losses and an appropriate external heat source. It is kept at around 300^{o} C to avoid any issues with respect to solidification. Mercury is liquid at room temperature but is not considered as a viable option as a coolant in this study due to its low boiling point (357^{o} C) and a relatively inferior thermal properties (thermal conductivity of 8.6 W/m-K and specific heat capacity of 139 J/kg-K) compared to Na.

	Na	Pb	LBE	He
Atomic Weight	22.997	207.21	208	4
Melting Point (°C)	97.8	327.4	123.5	n/a
Boiling Point (°C)	892	1737	1670	-267
Density (kg/m^3)	*880*	*10500*	*10300*	0.178
Specific Heat (J/kg-K)	*1300*	*160*	*146*	5200
Heat Capacity (MJ/m^3-K)	*1.14*	*1.68*	*1.50*	0.0009
Thermal Conductivity (W/m-K)	*76*	*16*	*11*	0.152 *0.238*
Viscosity (cP)	*0.34*	*2.0-2.5*	*1.7*	0.018 *0.031*

Values at STP. *Italic = Evaluated at ~300°C*

Table 3.3: Thermo-physical properties for fast reactor coolants [18]

As shown in Table 3.3, sodium has high specific heat and high thermal conductivity. Furthermore, the absorption cross section of sodium is low [2]. Hence, it doesn't contribute to parasitic absorption of neutrons. Moreover, coolant velocity could be easily managed if sodium is used as opposed to Lead Bismuth Eutectic (LBE) [18]. A higher coolant velocity is desirable due to the compactness of the core and a relatively low coolant volume fraction (7%).

3.5 Core homogenization

Using the volume fractions of fuel, cladding, structure and coolant, corresponding volumes occupied in each cell were calculated. Standard densities for these materials are used to calculate their masses in individual cell. Atomic weights are then used to compute the isotopic fractions of different nuclides in the cells. These isotopic fractions are used as input for MCNPX. For example, Table 3.4 lists the isotopic fractions of different materials in each cell in region A.

Isotopic fractions for cells in region B can be found by simply adjusting the enrichment level in uranium (0.7% enriched in ^{235}U for region B). These are shown in Table 3.5.

	Volume (cm^3)	Mass (g)	Isotopes	Isotopic fraction
Fuel (U-10 wt.% Zr)	13770	220467.34	^{235}U	0.211
			^{238}U	0.429
			^{91}Zr	0.185
Coolant (Na)	1134	1051.20	^{23}Na	0.035
Cladding and structural material (HT9)	1296	10018.08	^{56}Fe	0.116
			^{52}Cr	0.017
			^{59}Ni	0.001
			^{184}W	0.001
			^{96}Mo	0.001
			^{55}Mn	0.001
			^{28}Si	0.001
			^{51}V	0.001
			^{12}C	0.001

Table 3.4: Isotopic core composition of individual cell in the enriched region (Region A)

	Volume (cm^3)	Mass (g)	Isotopes	Isotopic fraction
Fuel (U-10 wt.% Zr)	13770	220467.34	^{235}U	0.004
			^{238}U	0.635
			^{91}Zr	0.185
Coolant (Na)	1134	1051.20	^{23}Na	0.035
Cladding and structural material (HT9)	1296	10018.08	^{56}Fe	0.116
			^{52}Cr	0.017
			^{59}Ni	0.001
			^{184}W	0.001
			^{96}Mo	0.001
			^{55}Mn	0.001
			^{28}Si	0.001
			^{51}V	0.001
			^{12}C	0.001

Table 3.5: Isotopic core composition of individual cell in the non-enriched region (Region B)

On the outside, the core is surrounded on all sides by reflector which is a homogenous mixture of HT9 and Na. It has 80% HT9 and 20% Na by volume.

3.6 Complete model

Figure 3.2 shows a sketch of the complete model generated using MCNP Visual Editor Version 22S.

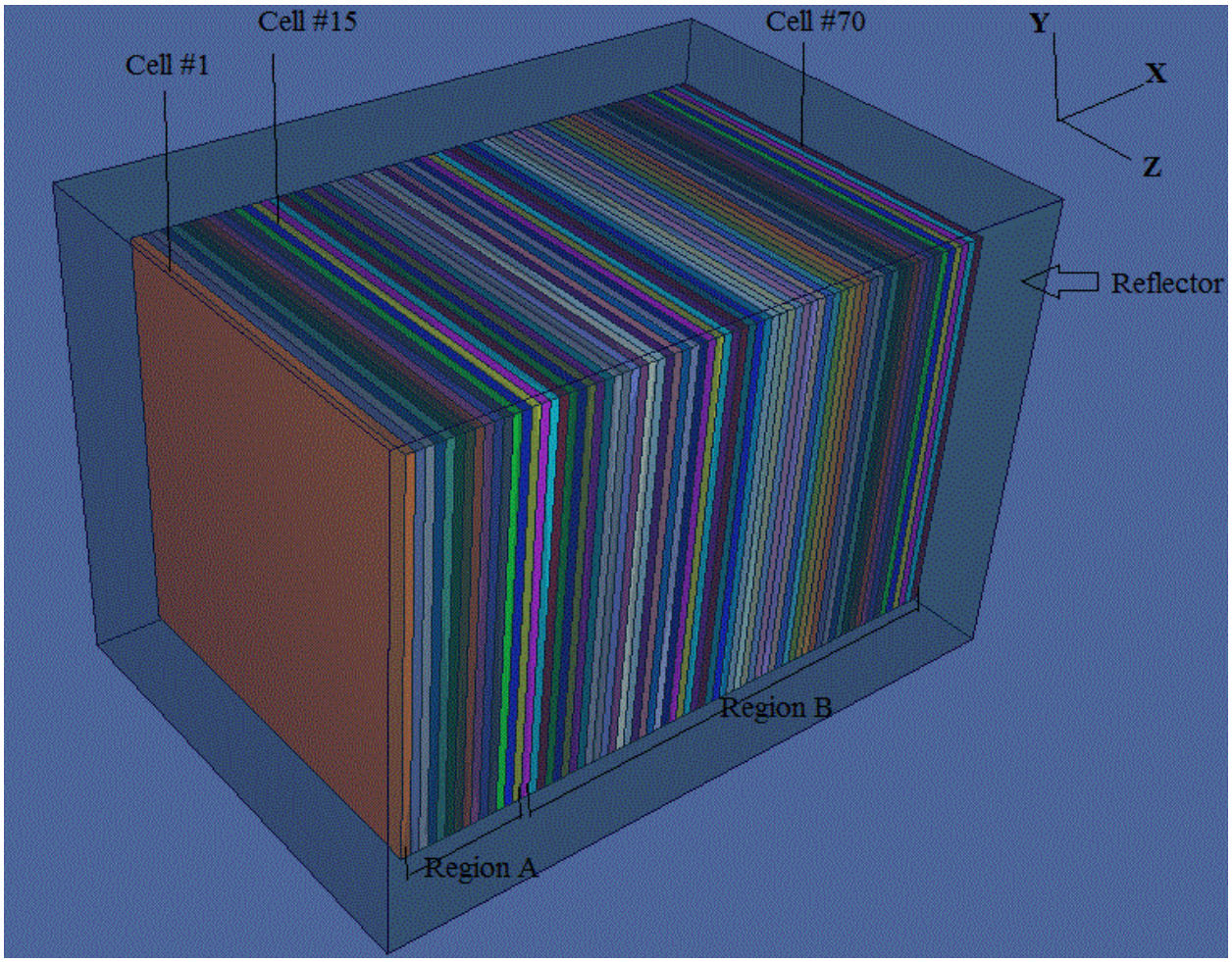

Figure 3.2: Core and reflector model of the TWR

3.7 Power level and reactor operation duration

Power level was specified as the normalization parameter for flux. The reactor was designed to operate at a constant thermal power of 350 MW. Operation at a fixed power level has implications on the evolution of flux profile over time. Specifically, it can impact the peak as well as the 'spread' of flux shape. Constant thermal power constraint should be kept in mind when comparing flux shapes at different times over the core life. The criticality and burn-up simulations were carried out to mimic reactor operation of 49 years. Results for evolution of flux shape and actinide inventories are presented in Chapter 4.

Chapter 4

Results and Analysis

Monte Carlo MCNPX v27c is used to simulate the core physics under specified power of 350 MW. A brief description and capabilities of the code are given in Appendix A. Setup of the TWR core for simulation in MCNPX is presented in section 4.1. Results and discussions are presented thereafter. First, an analysis of evolution of spatial flux profile over time is presented along with associated burn-up. Second, history of selected actinide inventories during core-life is presented. Finally, the wave speed is determined from the flux profiles.

4.1 Methodology

Volume averaged neutron flux is tallied for each cell in the model at various times. The cells are numbered in increasing order from 1 through 70 along the positive X-axis (see Figure 3.2). Each cell is assigned a homogeneous mixture of fuel, cladding, structural material and coolant with a specific isotopic concentration as described in sections 3.2, 3.3 and 3.4. Furthermore, the cells are enriched, as described in section 3.2.1.

Neutron flux in each cell is divided into 10 logarithmic energy groups; from 0 eV through 100 MeV. These groups are tabulated in Table 4.1. The purpose of this division is to compare the energy spectrum in the core. Moreover, for further analyses, all neutrons above 0.1 MeV are lumped into a single group henceforth referred to as fast group. In the following table, all neutrons in Group 1 through Group 3 are identically referred to as fast neutrons.

Energy	Group
0.0 eV – 0.1 eV	10
0.1 eV – 1.0 eV	9
1 eV- 10 eV	8
10 eV – 0.1 keV	7
0.1 keV – 1.0 keV	6
1.0 keV – 10 keV	5
10 keV – 0.1 MeV	4
0.1 MeV- 1.0 MeV	3
1.0 MeV – 10 MeV	2
10 MeV – 100 MeV	1

Table 4.1: Neutron energy groups

In this study, MCNPX simulations are carried out with 145 cycles (40 inactive cycles) with 10000 particles per history. The steady state (k) calculations are immediately followed by burn-up calculations in MCNPX. Convergence of k_{eff} in each steady state calculation is ensured by the 'normal distribution' at the 95 % confidence level for collision, absorption and track length estimate of k. Furthermore, the standard deviation for each batch of steady-state k_{eff} calculation is found to be less than 0.0006.

Time-steps are specified in the input deck for burn-up calculations. The first burn-up calculation is performed after 30 days of operation (to account for Xe buildup which starts accumulating after 2 days), and all subsequent burn-up calculations are carried out at time increment of 1200 days. Neutron fluxes in the cells are tallied at the end of each burn-up calculation.

Specific cells in the TWR core are chosen wherein the isotopic concentrations of the selected actinides are recorded throughout core lifetime. To facilitate the tracking of the selected isotopes, a nomenclature is proposed in Table 4.2 which will be used throughout this chapter. Isotopic evolution of ^{235}U, ^{238}U and ^{239}Pu are reported in this study.

Cells	Nomenclature for cell group (Zone)
1-5 (**L**eft end of core)	L
36-40 (**M**iddle of core)	M
66-70 (**R**ight end of core)	R

Table 4.2: Cell-group nomenclature

4.2 Space and time evolution of flux shape

The continuous breeding and burning of fissile materials gives rise to a shifting flux distribution in the core. This shift in the flux profile in the reactor core is analogous to the propagation of a wave, hence the term 'Traveling Wave Reactor'.

4.2.1 Initial total flux distribution in the core

The flux distribution at BOL is shown in Figure 4.1. The X-axis represents the cells in the model. (A reminder that flux magnitude is scaled in this and all subsequent flux plots such that the total thermal power is 350 MW.) As expected, the flux distribution is skewed and the peak is located at cell number 9 which lies in the enriched region to the right of the center of the enriched region. The flux drops rapidly towards the core end (right side in Figure 4.1) which consists of cells loaded with NU. The plot shows a relatively greater neutron population at the left end of the

reactor at BOL compared to the right end. This is due to the initial enrichment strategy. (Left end has fissile material whereas the remaining core merely has natural uranium as fuel.)

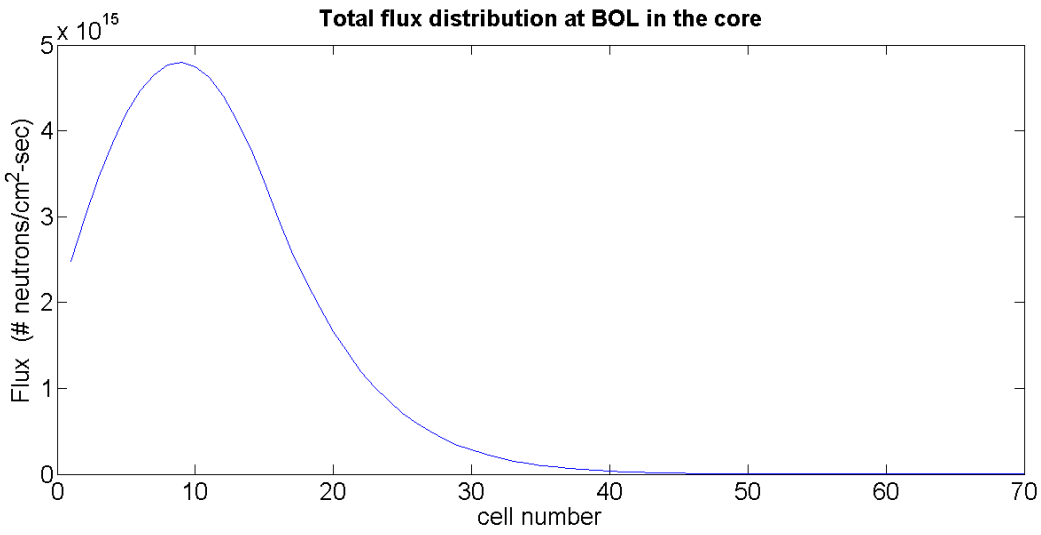

Figure 4.1: Total flux distribution at BOL

The presence of the reflector as an envelope around the reactor core prevents total flux at the left edge from dropping to near zero, as could be observed in Figure 4.1. In the absence of the reflector, we expect the flux at the edges to go to near zero due to the vacuum boundary condition.

4.2.2 Initial fast flux and thermal flux distribution in the core

We have defined fast flux as the flux of neutrons with energy greater than 0.1 MeV and thermal flux as one with energy less than 1 eV. Figure 4.2 shows the log plot of fast and thermal flux in the core at BOL. As seen from the figure, fast flux is about 1-3 orders of magnitude greater than the thermal flux. The difference between the fast flux and the thermal flux is maximum at the

location of the peak of the fast flux (around cell 9). The difference becomes progressively smaller as we traverse towards the right end of the core. However, fast flux is at about 10 times greater than thermal flux even at the location where the difference between them is the lowest (around cell 65).

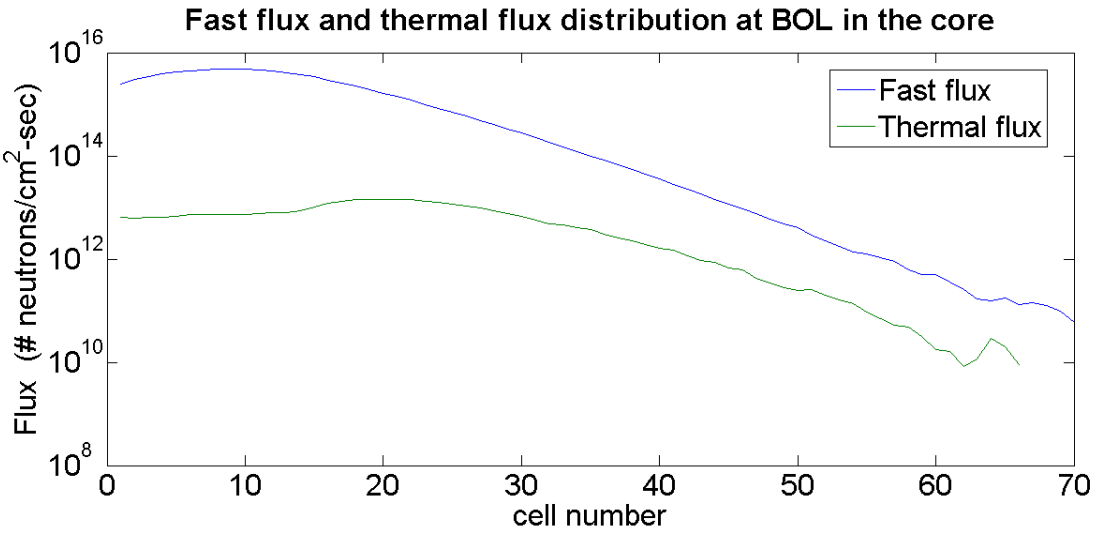

Figure 4.2: Fast flux and thermal flux comparison at BOL

Figure 4.3 shows the energy spectrum of neutrons at BOL. To calculate this, a separate simulation under the same initial conditions (same core dimensions, material compositions, enrichment levels etc.) was carried out. Neutron flux was divided into 52 logarithmic energy bins between 0 eV and 100 MeV. Each energy group was added over all 70 cells and averaged, thus generating the core-averaged energy spectrum of Figure 4.3. The neutron spectrum at BOL in the TWR core, as expected, is in the fast energy range (E > 0.1 MeV). In essence, the total flux is sufficiently represented by fast flux alone, as seen in Figure 4.4.

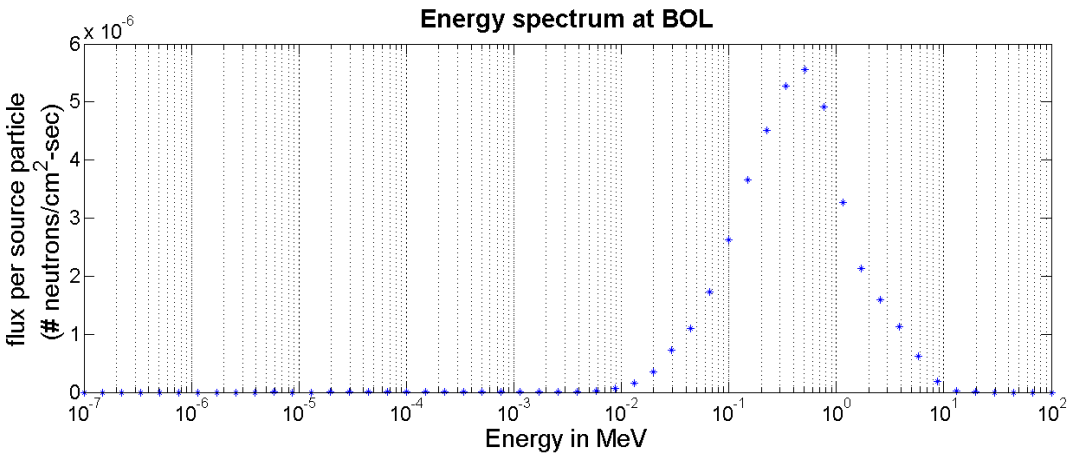

Figure 4.3: Energy spectrum at BOL

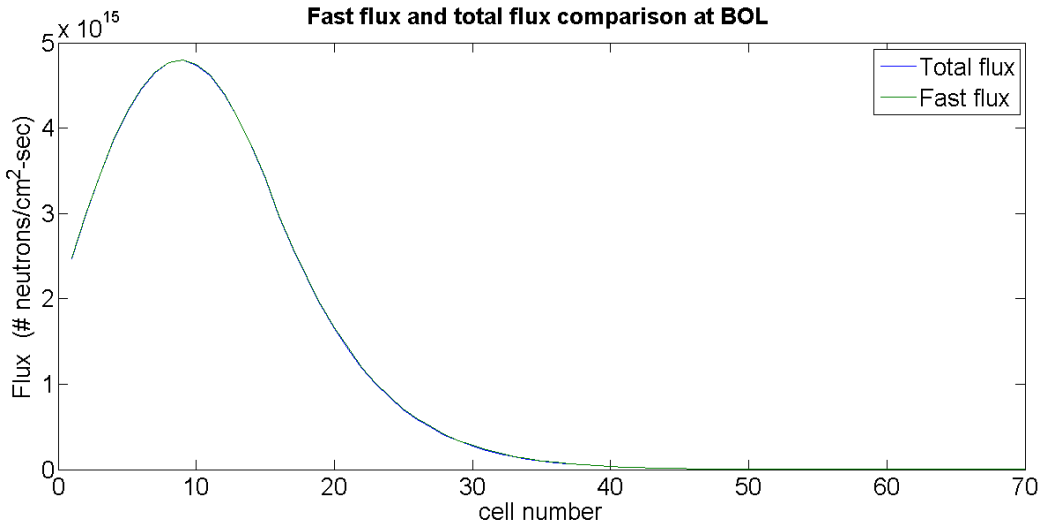

Figure 4.4: Total flux and fast flux at BOL

The hard spectrum is primarily due to the lack of moderating material in the core. Sodium coolant does not act as a good moderating material like water in Light Water Reactors (LWRs). Subsequently, most fission reactions are caused by fast neutrons alone. The low fast fission cross-section of the fissile materials is compensated by the high flux levels in the core as observed in Figure 4.2 and Figure 4.3.

4.2.3 Fast flux evolution in the core

It was hypothesized that the initial flux distribution maintains its overall shape but shifts gradually to the region of less enrichment (breeding region) throughout the operation period. Figure 4.5 shows the space and time evolution of fast flux over core lifetime of nearly fifty years. The flux profile moves like a wave towards the right with time. From the figure, it is seen that the flux profile spreads out over the core with time compared to BOL. This is due to the requirement of operation under constant power.

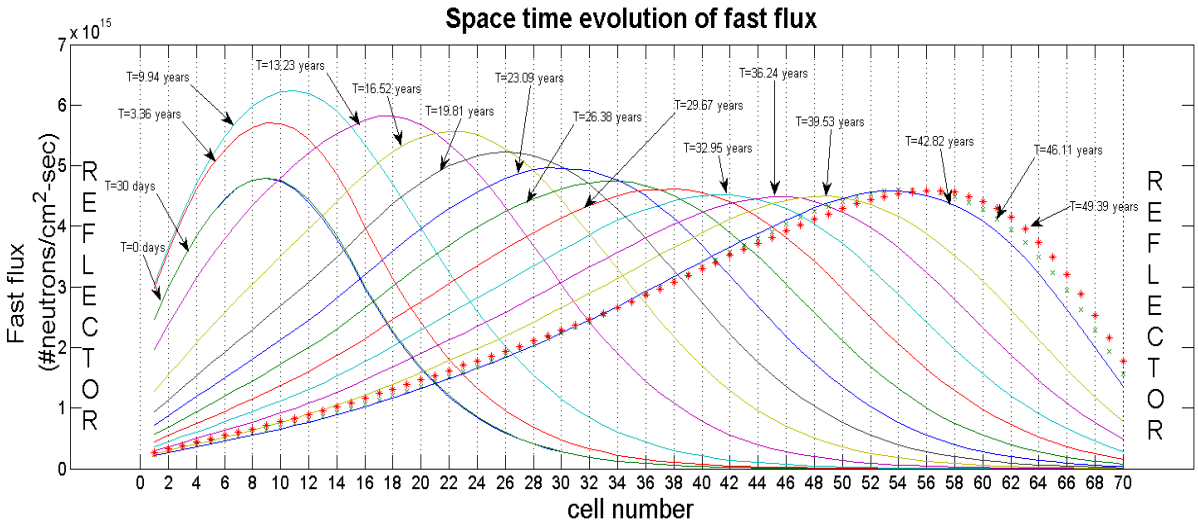

Figure 4.5: Space-time evolution of fast flux

Excess reactivity at BOL (t = 0 days, k_{eff} = 1.39) accelerates breeding of fissile isotopes at startup. Xe buildup during the first thirty days increases the rate of absorption of neutrons and reduces the excess reactivity. Between t = 0 days and t = 3.36 years, ^{239}Pu is produced according to the conversion chain of Figure 1.1. Neutron yield per neutron absorbed (η) for ^{239}Pu is higher than that for ^{238}U. The flux varies according to the evolution of local isotopic composition. The flux at t = 3.36 years is found to be larger than that of t = 0 days. It increases till t = 6.65 years after which it gradually decreases.

The peak in flux profile steadily decreases and moves to the right between 6.65 years and 26.38 years. After 26.38 years, the peak value for the flux distributions is fairly constant till the end of simulation (t = 49.3 years). It can also be observed that the wave speed for the peak is slightly larger for the first half of the core life than for the second half. This slowing down in wave speed is attributed to the continuously decreasing breeding region in the second half of the core. Additional analyses on wave speed are presented in Section 4.5.

It is interesting to note that the flux between cell #1 and cell #30 (the enriched region at t = 0) for t = 46.11 years and t = 49.39 years is greater than that for t = 42.82 years. This increase in flux in the first 30 cells is contrary to the trend of decreasing flux for 10 years < t < 33 years. This reversal is also the result of the constraint of constant thermal power during core operation.

4.3 Core reactivity

Values of core multiplication factor k_{eff} are shown in Table 4.3 at several times. The initial excess reactivity is required to compensate for the production of poisons in the first burn step. By trial and error, the initial isotopic concentrations were chosen such that the core remained close to critical over core life, which is about 43 years. It is seen that the multiplication factor decreases till about t = 9.94 years. The instance when $k_{eff} < 1$ (a little before t = 9.94 years), the reactor will (become subcritical and) shut down. This is a shortcoming of this particular design and initial enrichment level. Ideally, the core should not "pre-maturely" go subcritical. The problem can be alleviated by simply starting from a slightly higher enrichment level or by using a larger core. However, as can be seen from Table 4.3, if the breeding continues, the multiplication factor increases back to above one, and then stays above one for more than 20 years. Note that breed-and-burn design reactors are expected to operate with multiplication factor very close to one (little excess reactivity), and hence it is quite likely that due to some reason they may become subcritical. Hence, there should be a mechanism built in these reactors to sustain the chain reaction for the period when $k_{eff} < 1$, until it comes back to unity due to

breeding. Since with $k_{eff} < 1$, these reactors look very much like accelerator driven system, it is possible to operate the reactor as a driven system using an external source of neutrons in the unforeseen case of k_{eff} falling below one. Such subcritical systems have been proposed by van Dam [19] and Fomin [12]. They modeled an external neutron source to induce breeding at startup and hence make the core critical. For t > 9.94 years, a gradual increase in the multiplication factor can be seen till t = 29.67 years. This is attributed to the combined effect of relative decrease in neutron leakage from the edges and buildup of fissile materials in the inner core. A monotonous decrease in the multiplication factor is seen for t > 29.67 years till the end of core life (t = 42.8 years). Two additional batches of steady-state calculations are carried out (when $k_{eff} < 1$) and are shown in italics in Table 4.3.

Time in days	Time in years	k_{eff}
0	0	1.392
30	0.08	1.386
1230	3.36	1.194
2430	6.65	1.005
3630	9.94	0.97
4830	13.23	1.001
6030	16.52	1.002
7230	19.81	1.034
8430	23.09	1.037
9630	26.38	1.040
10830	29.67	1.040
12030	32.95	1.038
13230	36.24	1.033
14430	39.53	1.024
15630	42.82	1.008
16830	*46.11*	*0.985*
18030	*49.39*	*0.958*

Table 4.3: History of k_{eff} during core life

4.4 Burn-up and power fraction

In this section, results of overall burn-up in the core at various stages of operation are presented. Burn-up is a quantitative measure of amount of energy extracted from the fuel per unit mass. Table 4.4 shows cumulative burn-up in the core at the end of prescribed time steps. Due to the constant thermal power constraint, burn-up in each time interval is essentially constant (= 30 GW-days/MTU). Burn-up of 394 GW-days/MTU is observed at the end of critical life. It is comparable to the 400 GW-days/MTU discharge burn-up reported by Sekimoto in the CANDLE reactor [11]. Furthermore, since the flux is not constant with respect to time and space, burn-up at various locations in the core is not uniform. To this end, analyses of burn-up at specific locations in the core were carried out and the results are presented.

Time in days	Time in years	Burn-up (GWd/MTU)
0	0	0
30	0.08	7.56E -01
1230	3.36	3.10E+01
2430	6.65	6.12E+01
3630	9.94	9.15E+01
4830	13.23	1.22E+02
6030	16.52	1.52E+02
7230	19.81	1.82E+02
8430	23.09	2.12E+02
9630	26.38	2.43E+02
10830	29.67	2.73E+02
12030	32.95	3.03E+02
13230	36.24	3.33E+02
14430	39.53	3.64E+02
15630	42.82	3.94E+02
16830	*46.11*	*4.24E+02*
18030	*49.39*	*4.54E+02*

Table 4.4: History of burn-up

Three primary zones were chosen according to Table 4.1 to analyze local burn-up. Zone *L* is composed of cells 1 through 5. Zone *M* is the middle portion of the reactor and is composed of cells 36 through 40. Zone *R* is the rightmost part of the reactor and is composed of cells 65 through 70. Burn-ups for zone *L*, zone *M* and zone *R* at various times are presented in Figure 4.6, Figure 4.7 and Figure 4.8, respectively.

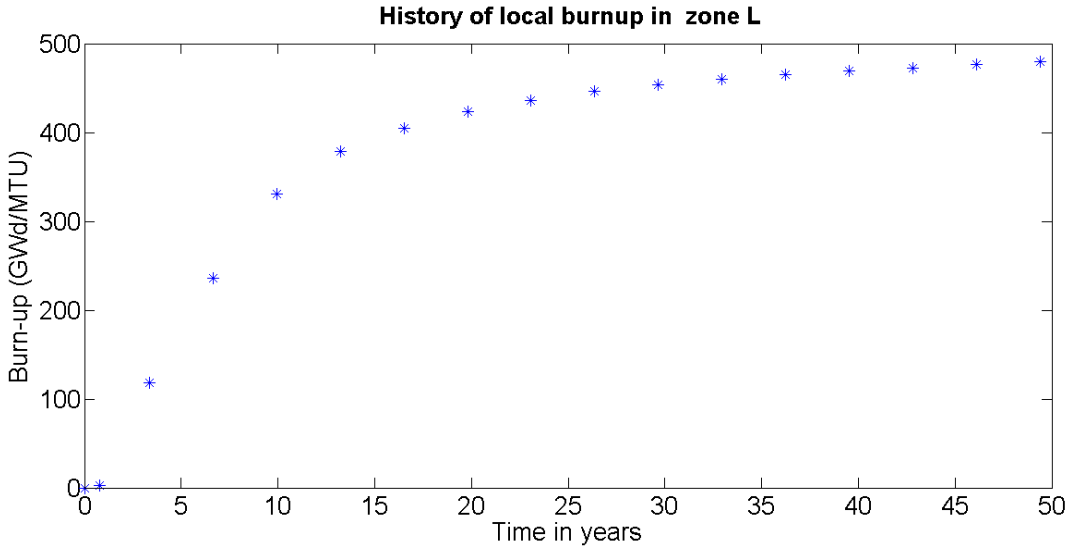

Figure 4.6: Cumulative burn-up in Zone *L*

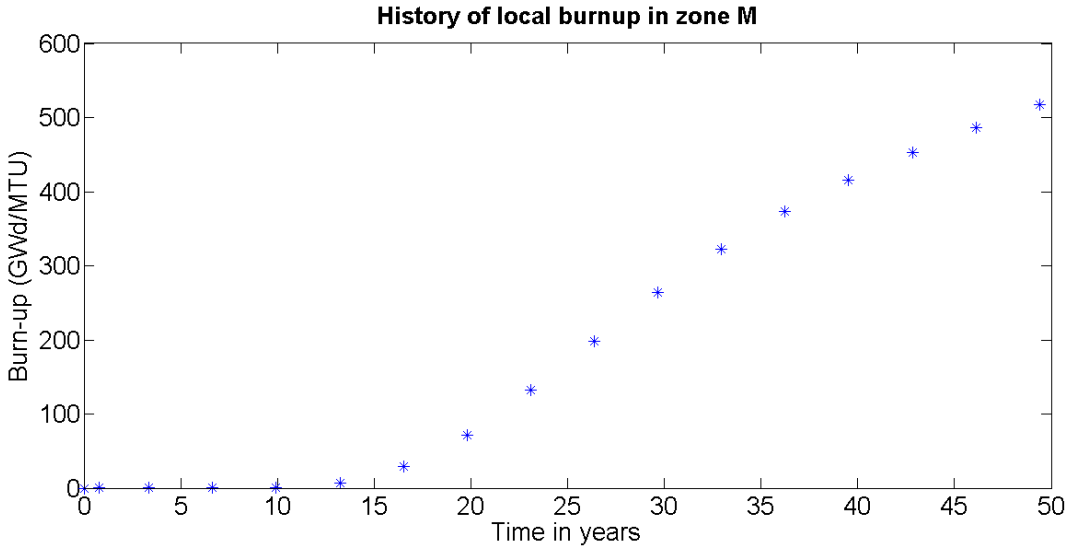

Figure 4.7: Cumulative burn-up in Zone *M*

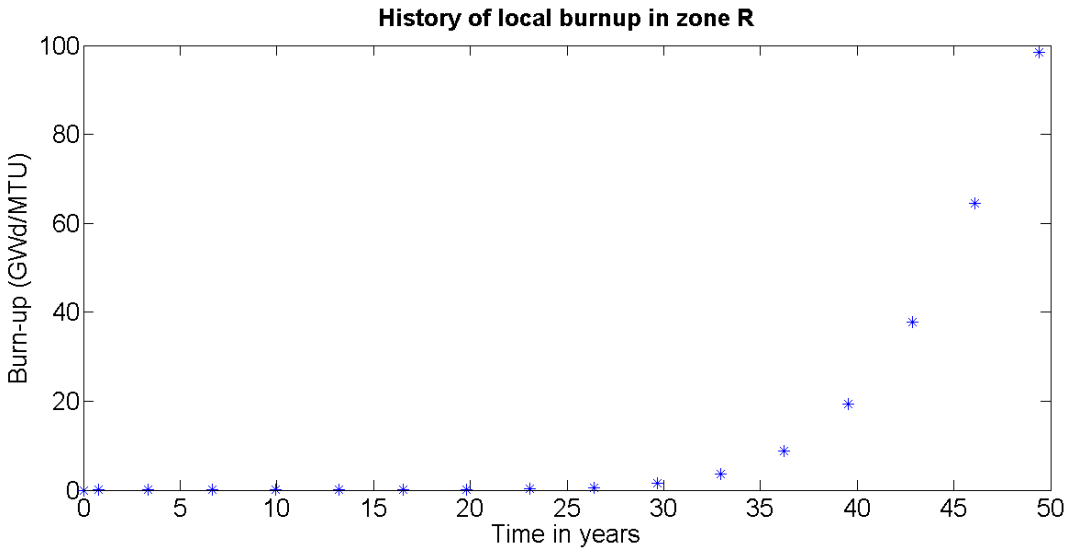

Figure 4.8: Cumulative burn-up in Zone *R*

In zone *L*, it is observed that burn-up rate is highest at initial stages of reactor operation. The presence of enriched fissile material along with a high fast flux induces maximum burn-up rate in the initial stages. Furthermore, the rate of increase of burn-up in zone *L* continuously decreases after t = 30 days, as could be seen from the decreasing slope between adjacent data points in Figure 4.6. This is explained by the location of peak of fast flux at various times over core-life. BOL corresponds to peak location towards the left end and hence burn-up rate is higher. As the peak shifts towards the right of the core at latter stages, rate of increase of burn-up in zone *L* slows down and hence we see the plateau at latter time steps in Figure 4.6.

In zone *M* which corresponds to the middle of the reactor, burn-up is virtually zero till about 13 years, after which a rapid increase in burn-up is observed. The maximum burn-up rate occurs in years $23.09 < t < 26.38$ years. Moreover from Figure 4.5, we can see that the peak for flux distribution corresponding to t = 26.38 years falls in the middle of the core, viz. zone *M*, hence the maximum burn-up rate.

Similarly, burn-up in zone *R* kicks off when the flux peak has reached the right end of the reactor. From Figure 4.8, this corresponds to 30 years. A quick look at Figure 4.5 confirms the observation.

Power fraction at a specific location is directly related to burn-up at that location. A higher burn-up rate corresponds to a higher power fraction. In Figures 4.6, 4.7 and 4.8, cumulative burn-up at specified locations in the core were plotted versus time. The time-space corresponding to the maximum slope in the aforementioned plots corresponds to the maximum power fraction in a given region. Figures 4.9, 4.10 and 4.11 show power fractions for zone *L* zone *M* and zone *R* plotted versus time. As seen in these plots, the peaks correspond to the maximum slopes for Figures 4.6, 4.7 and 4.8, respectively.

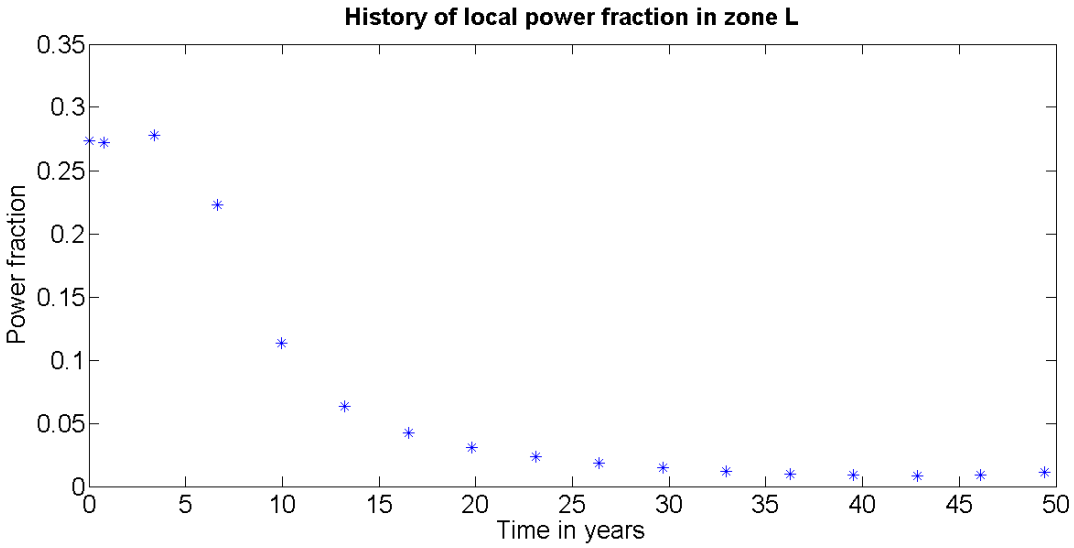

Figure 4.9: History of power fraction in Zone *L*

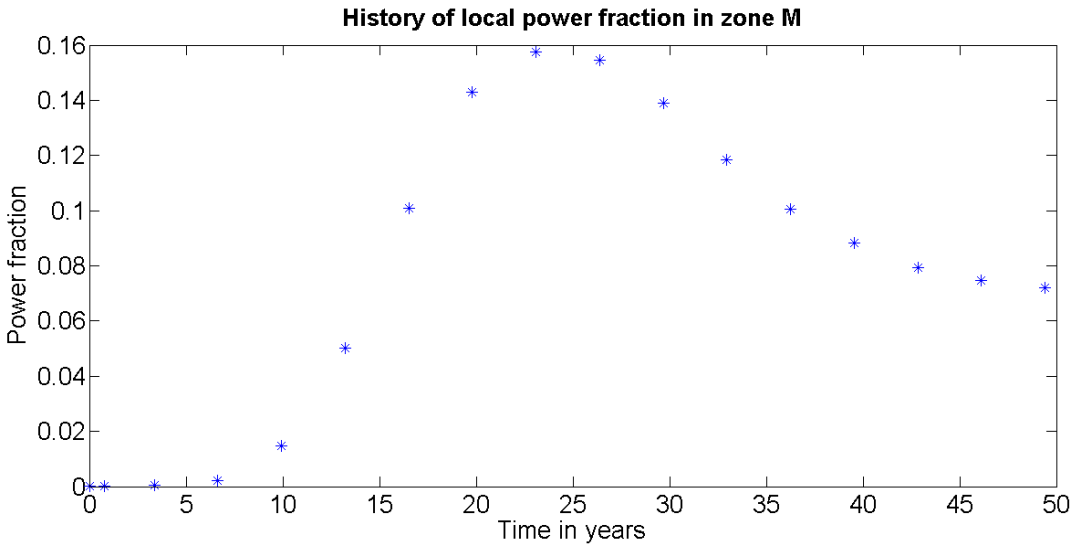

Figure 4.10: History of power fraction in Zone *M*

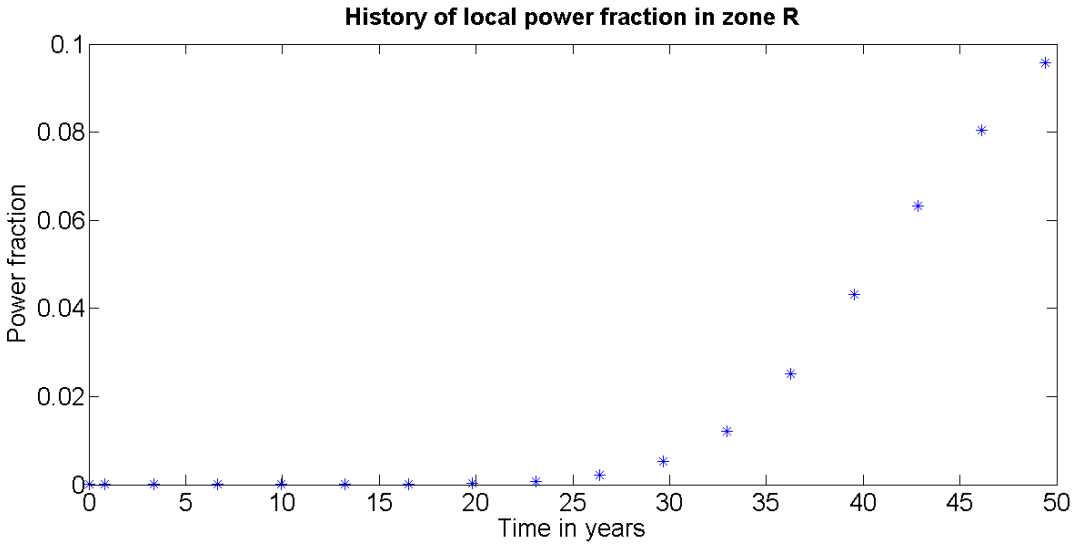

Figure 4.11: History of power fraction in Zone *R*

4.5 Traveling wave speed calculation

An analysis of overall speed of the shift in flux distribution, henceforth referred as wave speed, is presented in this section. Figure 4.5 is used to approximate the speed of the traveling wave. The peak locations of flux distribution at various times are noted, beginning at t = 30 days and ending at t = 42.82 years. The differences between peak-locations for adjacent time steps for all 14 flux profiles, 1 of which is not shown in Fig. 4.2.3, are averaged. This is then divided by the uniform time duration which is 1200 days in this study. The resulting speed is found to be about 2.11 cm/year. This is consistent with results reported in literature, which varies from 2 cm/year to 7 cm/year [11, 12, 13]. The relatively lower speed is due to the use of 'dense' core for the analysis, i.e. the volume and weight fractions for fuel were relatively higher for the simulation compared to other proposed designs. This average wave speed may however be a bit misleading. As can be seen in Fig. 4.2.3, the wave travels faster, with an average speed of 2.66 cm/year, during the early life of the core (6.65 years < t < 32.95 years), but slows down to some extent towards the end of core life (32.95 years < t < 42.82 years). Its average speed for 32.95 years < t < 42.82 years is calculated to be only 1.6 cm/year. It can also be observed that the slower wave speed towards the end of life corresponds to the time period during which the multiplication factor continuously decreases (see Table 4.3). A summary of peak locations of various flux profiles versus time are shown in Table 4.5.

Flux distribution at time T =	Location of peak (Cell #)	Location of peak (x in cm)
30 days	9	18
3.36 years	10	20
6.65 years	11	22
9.94 years	18	36
13.23 years	22	44
16.52 years	26	52
19.81 years	30	60
23.09 years	34	68
26.38 years	38	76
29.67 years	42	84
32.95 years	46	92
36.24 years	49	98
39.53 years	52	104
42.82 years	54	108

Table 4.5: Peak locations of flux versus time

4.6 Actinide inventories

MCNPX keeps a record of all the isotopes formed during the operation of the reactor. However, the inventory of only selected actinides is presented in this study. First, a study of relative abundance of ^{235}U, ^{238}U and ^{239}Pu over time is presented in this section. Then, section 4.6.1 presents the relative abundance of the aforementioned actinides in zone *L*, zone *M* and zone *R* as explained in the previous section. Finally, section 4.6.2 presents an overview of the main actinides and non-actinides at the end of life (EOL).

Figure 4.12 and Figure 4.13 show a history of main nuclides in the core by mass fraction (of total mass) and total mass, respectively. A general trend in the consumption of fertile materials and production of fissile materials could be seen in Figure 4.12 and Figure 4.13. The total amount of ^{238}U steadily decreases in the core by breeding ^{239}Pu. ^{239}Pu does not increase by the same amount ^{238}U decreases mainly because some ^{239}Pu is consumed in fission reactions immediately after its production. This tandem process of breeding and burning of fissile isotopes sustains criticality in the core.

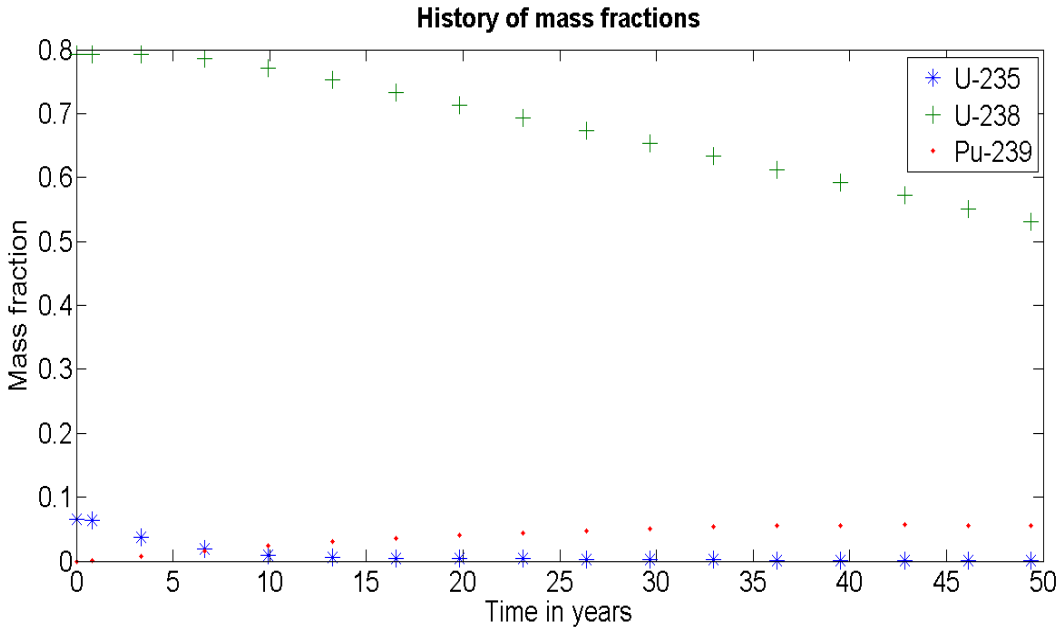

Figure 4.12: History of mass fractions for selected nuclides in the core

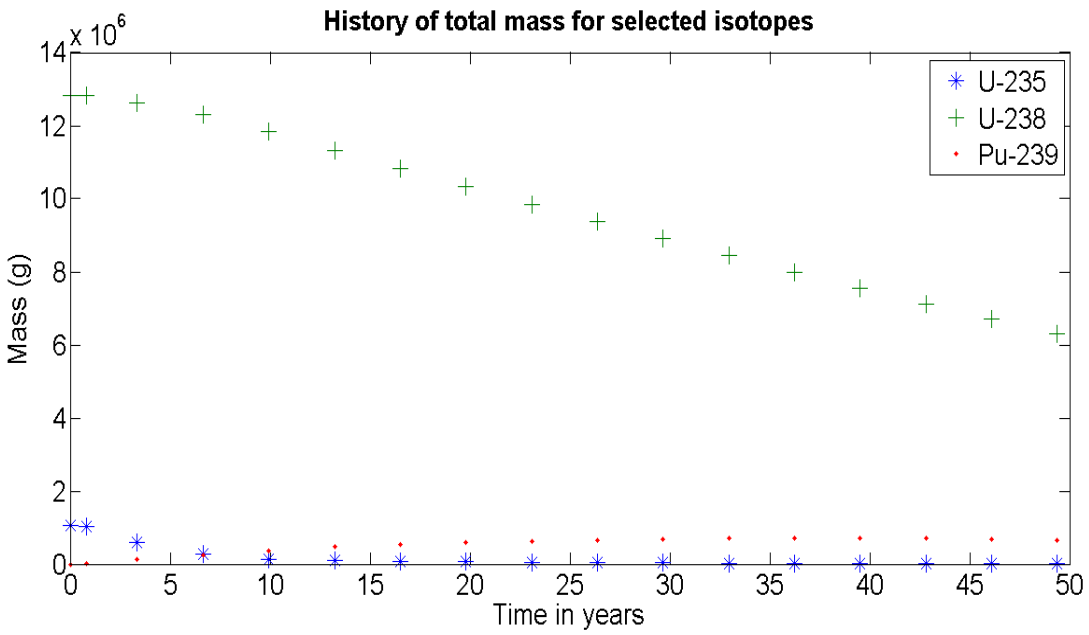

Figure 4.13: History of total mass for selected nuclides in the core

4.6.1 Listing by zones

Total mass of ^{235}U, ^{238}U and ^{239}Pu are plotted in Figures 4.14, 4.15 and 4.16 for zones *L*, *M* and *R*, respectively.

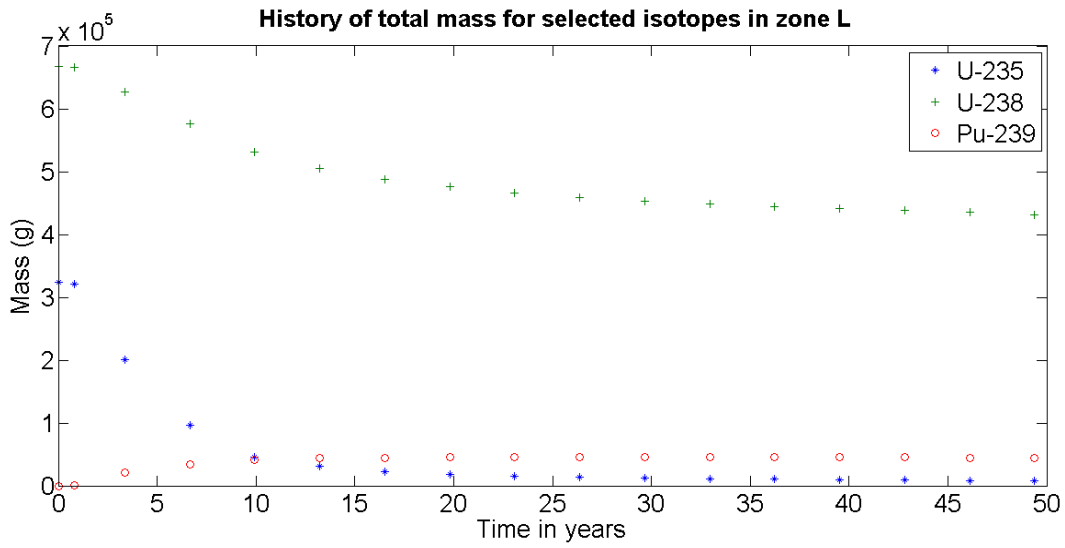

Figure 4.14: History of total mass for selected nuclides in zone *L*

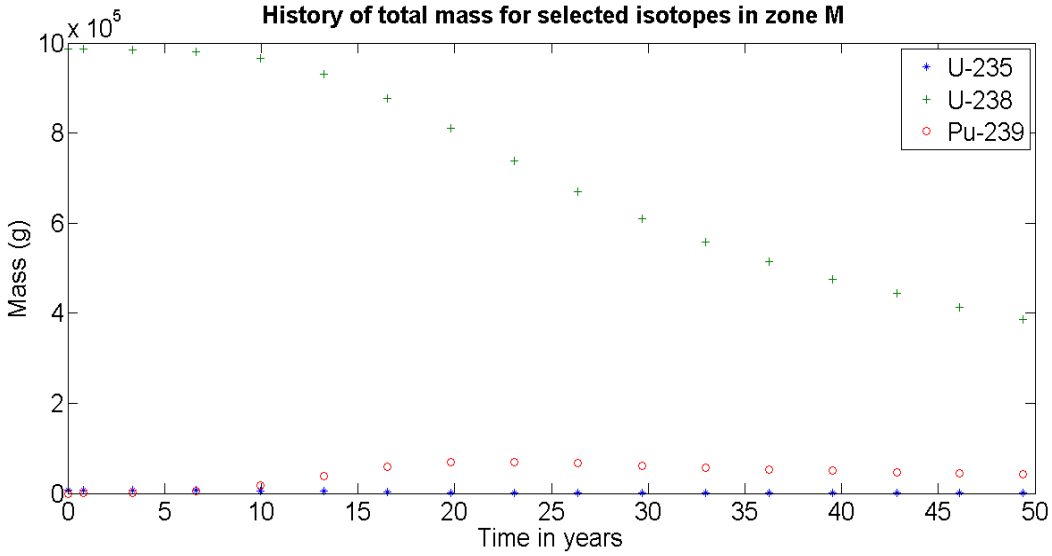

Figure 4.15: History of total mass for selected nuclides in zone *M*

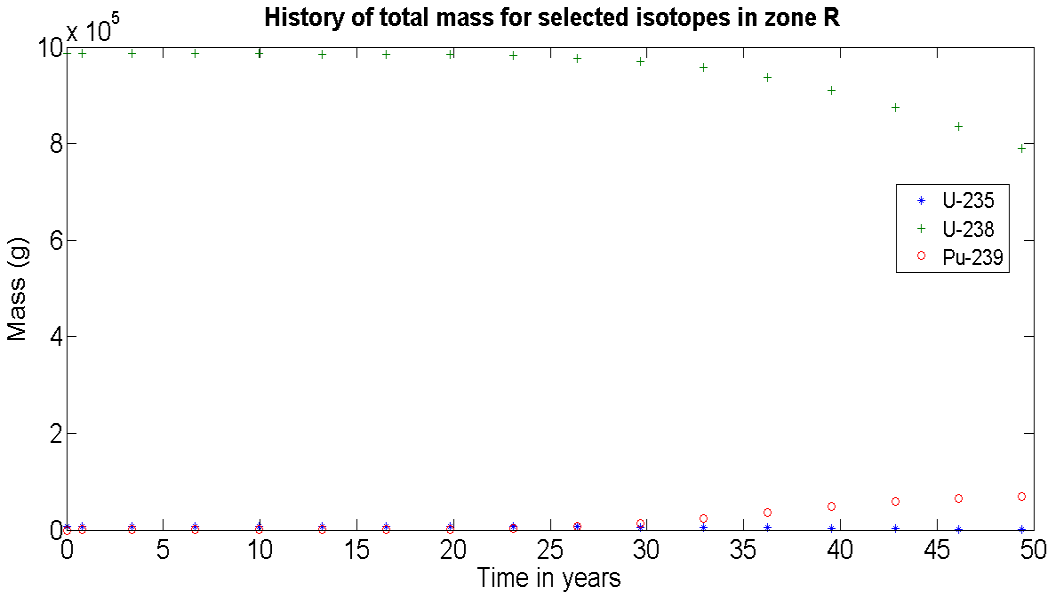

Figure 4.16: History of total mass for selected nuclides in zone *R*

As we can see from Figure 4.14, at BOL, there is a sharp decrease in concentration of ^{235}U. The fission of ^{235}U in zone *L* at BOL supports criticality of the core while U-238 is being converted to ^{239}Pu by (n, γ) reaction. The production of ^{239}Pu at BOL can also be observed. Towards EOL, the production of ^{239}Pu in zone *L* saturates. Figure 4.15 shows the same general trend for ^{239}Pu and ^{238}U as observed in Figure 4.14 but the onset of production of ^{239}Pu (equivalently loss of ^{238}U) is delayed when compared to that for zone *L*.

Figure 4.16 shows the analyses for zone *R*. At BOL, it is observed that there is virtually no activity for any of the isotopes. This is due to the fact that the wave only reaches zone *R* towards EOL. At EOL when the wave reaches zone *R*, a drop in concentration of ^{238}U, accompanied by production of ^{239}Pu could be seen.

4.6.2 End of life

Effective actinide management at EOL has been a focus of GNEP. To this end, inventories for major actinides are presented in Table 4.6. A study of EOL inventory is necessary for reprocessing and long-term storage purposes.

Isotopes	Mass (g)
^{232}Th	0.1230
^{233}Pa	0.0006
^{234}U	2655
^{235}U	12610
^{236}U	71180
^{237}U	42.3100
^{238}U	6712000
^{239}U	6.2760
^{236}Np	3.8280
^{237}Np	26080
^{238}Np	10.1300
^{239}Np	905.4000
^{236}Pu	0.0898
^{237}Pu	0.1126
^{238}Pu	16470
^{239}Pu	683600
^{240}Pu	192400
^{241}Pu	18090
^{242}Pu	6800

Table 4.6: EOL actinide inventory

Chapter 5

Core Thermal-Hydraulics

This chapter presents a simplified thermal-hydraulics analysis for the TWR core. First, the operating conditions are discussed and assumptions are listed. First order calculations are carried out to determine associated parameters like nominal flow rate, suggested operating temperatures etc. Owing to the asymmetric and time-evolving flux shape, a time dependent algorithm for heat extraction from the core is suggested. Then, a sample calculation is presented to illustrate the proposed algorithm. Possible design and control for coolant inlet through the bottom grid plate of the core are discussed. Finally, challenges of using sodium as a coolant are briefly outlined.

5.1 Operating conditions and assumptions

A homogeneous core was considered in the previous Chapter for neutronics analyses. To proceed with the analysis of the heat removal mechanism from the core, a 'uniformly heterogeneous' core is considered. Uniform heterogeneity here simply refers to a uniform core in which the coolant flows in between and parallel to the fuel pins. For example, fuel pins may be arranged in a hexagonal tight-packing orientation such that three fuel pins form a triangular flow channel among them. A sketch is shown in Figure 5.1. By implementing a 'uniformly heterogeneous' scheme, axially oriented flow channels parallel to the Y direction (see Figure 5.2) can be used for preliminary TH analyses. (Note: The triangular lattice is the typical arrangement of fuel pins in a fast reactor. Typical pin pitch-to-diameter ratio for a fast reactor is about 1.06 [13]. In-depth TH analysis in the other two directions in such an arrangement is not covered in this thesis.) As mentioned in section 3.4, the coolant volume is assumed to be 7% of the total core volume. In the analysis in this section, mixing of sodium in the core is allowed. (Section 5.2 presents analyses on controlled coolant flow through prescribed flow zones where sodium mixing is prohibited.)

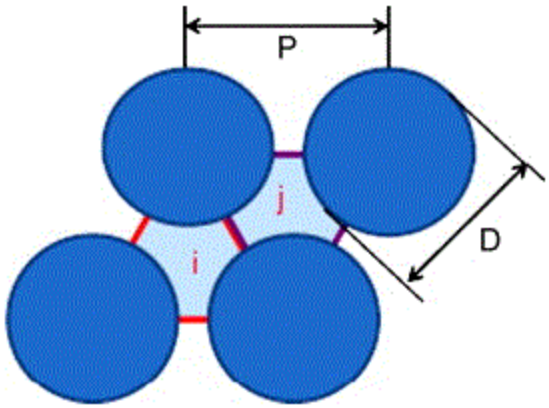

Figure 5.1: Sketch of triangular coolant channels [20]

The coolant flow is in a direction perpendicular to the direction of wave propagation. For example, in Figure 5.2, if the wave propagates in the positive X direction, the coolant flow is either in the Y or Z direction. We here consider the flow to be in the positive Y direction as shown in Figure 5.1.

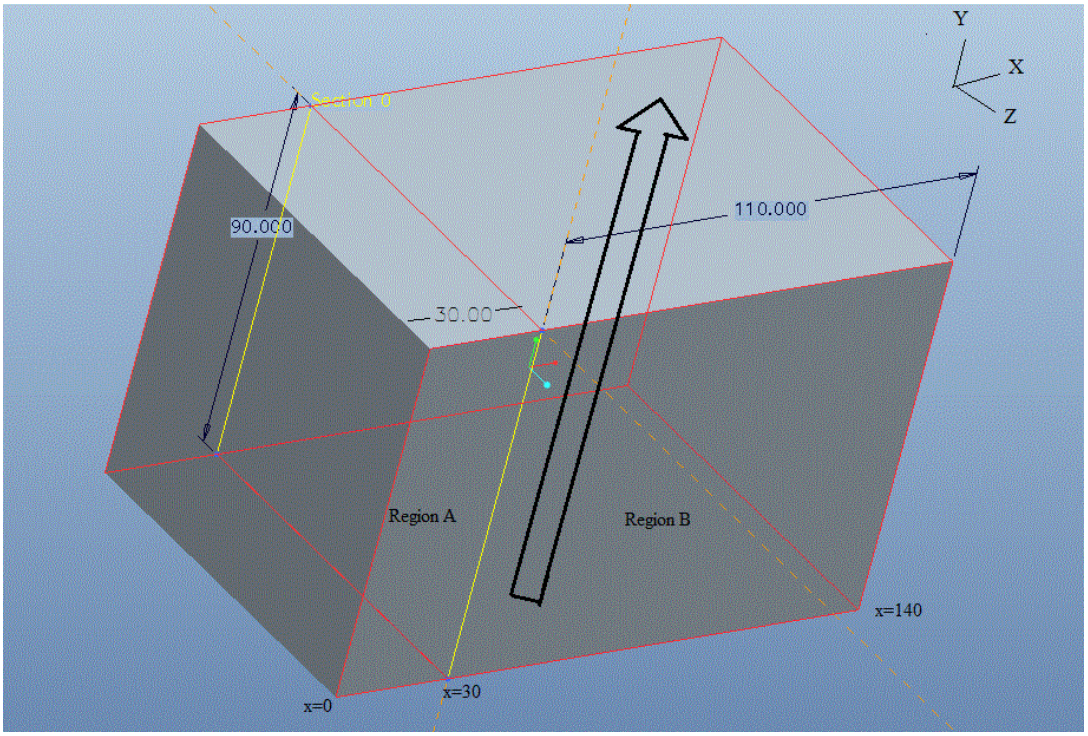

Figure 5.2: Schematic direction of coolant flow (dimensions are shown in cm)

Thermal-hydraulics conditions for the core-averaged conditions are presented first. (A refined model for coolant flow is presented in Section 5.2.) Under a constant thermal power and prescribed temperature change, average coolant flow rate through the core is calculated using Equation 5.1.1.

$$\dot{Q} = \dot{m}\ c\ \Delta T \tag{5.1.1}$$

Where,

$\dot{Q} = Heat\ generated\ (and\ removed)\ per\ unit\ time\ (thermal\ power) in\ units\ of\ \frac{J}{sec}$

$c = Specific\ heat\ capacity\ of\ sodium\ in\ units\ of\ \frac{J}{kg.K}$

$\Delta T = Difference\ between\ outlet\ and\ inlet\ temperature\ in\ units\ of\ K$

$\dot{m} = Coolant\ flow\ rate\ in\ units\ of\ \frac{kg}{sec}$

Using cross sectional area for coolant flow (7% of 90 × 140 cm^2 i.e. 0.0882 m^2) and the density of sodium (880 kg/m^3), average axial flow velocity is calculated from Equation 5.2.2.

$$\dot{m} = \rho\ v\ A \tag{5.2.2}$$

Where,

$v = Average\ axial\ flow\ velocity\ (\frac{m}{\sec})$

$A = Cross\ sectional\ area\ for\ coolant\ flow\ (m^2)$

$\rho = Density\ of\ sodium\ (\frac{kg}{m^3})$

Table 5.1 lists the basic operating conditions of the core calculated using this approximation.

Thermal power ($\dot{Q}$)	350 MW
Primary coolant	Sodium
Specific heat capacity of sodium (c)	1300 J/kg-K
Density of sodium (ρ)	880 kg/m^3
Suggested core inlet temperature	300^{o}C
Suggested core outlet temperature	600^{o}C
ΔT	300^{o}C
Average coolant flow rate ($\dot{m}$)	897.4 kg/sec
Average coolant velocity (v)	11.5 m/sec

Table 5.1: Suggested thermal-hydraulics operating conditions for TWR core

The calculated core-averaged coolant velocity is slightly high owing to the use of a compact core with a low coolant volume fraction (7 %). However, reported coolant volume fraction in other designs is around 30% [13, 14]. Assuming other parameters like total dimensions, power and ΔT remain the same, a 30% coolant volume fraction in the current design yields an average flow velocity of 2.7 m/sec (compared to 11.5 m/sec obtained with current volume fractions). Viable flow velocity as high as 8.3 m/sec has been reported for sodium cooled fast reactors [18]. Chang and Pinto et al. reported an average coolant velocity of 1.6 m/sec in their ANL report on design of modular sodium-cooled fast reactors [13]. It should also be noted that the dimensions and operating power level for a sodium cooled fast reactor design are higher than those used in this study. Fomin et al. reported a cylindrical core of radius 220 cm and height 500 cm with a coolant volume fraction of 30%. The power level in his design was varied between 2.3 GW and 3.9 GW [12].

A larger core size and an increased coolant volume fraction will result in a lower flow velocity than that reported in Table 5.1.

5.2 Recommended flux-profile-adjusted heat removal mechanism

Ideally, the coolant flow rate through the channels should be adjusted such that the maximum flow occurs in the region with the highest power density. A profile of local power fraction at any given time in the core is given by the flux shape at that time. For better thermal-hydraulics analyses, it is recommended that the core be divided into 14 zones in the X direction; with each zone containing 5 adjacent cells. For example, cells 1 through 5 could be in zone I, cells 10 through 15 could be in zone II, and so on. These zones could serve as individual flow channels wherein the flow rate is controlled independently. No sodium mixing is allowed between the adjacent coolant zones. It should be noted that the inlet temperature for all the flow channels is the same and is set to 300^{o} C. This will ensure no solidification of sodium occurs in zones where power fraction is low. The power fraction in each zone at any given time can be used to calculate the coolant flow rate for that zone. This space and time dependent flow will not only minimize unnecessary costs of pumping but will also serve to minimize erosion in the core over its lifetime.

A sample calculation is carried out to illustrate the proposed scheme. A specific time is chosen, say t = 13.23 years. Using the local power fractions in the core at t = 13.23 years, corresponding local power specific to each zone is found. These are given in Table 5.2. Each zone is then treated as a miniature core. Mass flow rate and flow velocity for each zone are then calculated as described in Section 5.1 (with the same desired ΔT). Results for the coolant flow profile in the core for t = 13.23 years is shown in Figure 5.3. It is seen that the overall shape of the profile, as expected, is very similar to the shape of the flux distribution in the core at t = 13.23 years (Figure 4.5). This is due to the direct correlation between the flux profile and the power density profile. A higher flux corresponds to a greater power density, and hence a greater flow rate. Equivalently, if we were to plot the flow profile at any other time, we can expect a shape similar to the corresponding flux profile at that time.

Cell Groups	Local Power (MW)
1-5	22.12
6-10	28.86
11-15	39.95
16-20	63.77
21-25	70.45
26-30	61.00
31-35	38.71
36-40	17.53
41-45	6.05
46-50	1.77
51-55	0.52
56-60	0.15
61-65	0.05
65-70	0.04

Table 5.2: Local power in the TWR core at t = 13.23 years

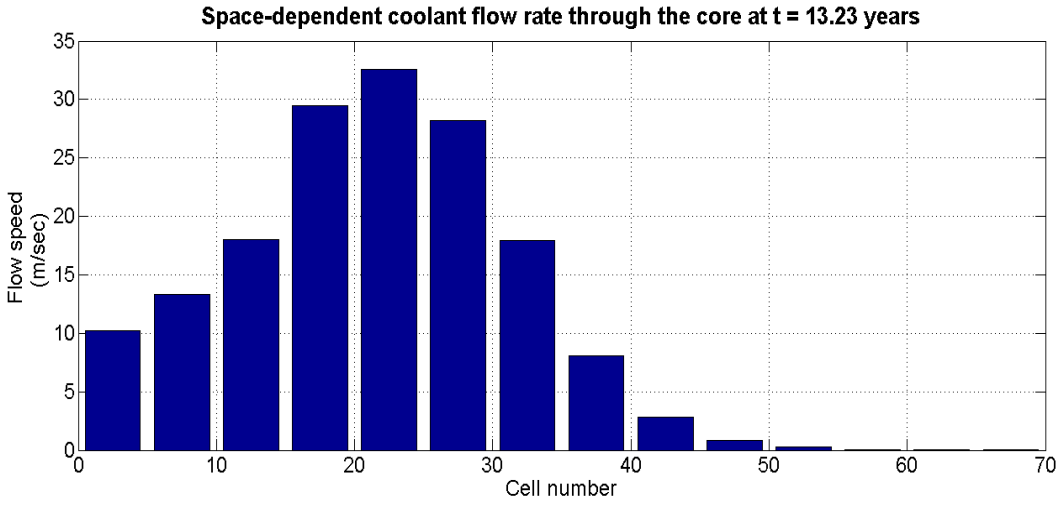

Figure 5.3: Space-dependent coolant flow rate at t = 13.23 years

A peak velocity of about 33 m/sec is observed for Cell #21 through Cell #25 in Figure 5.3. This is obviously very high. But it should be noted that, following the discussions in the previous section, the data presented in the above figure will be scaled down in an actual TWR design by as much as a factor of four or five. Figure 5.3 primarily illustrates the idea of flux-adjusted, space-dependent coolant flow algorithm. The absolute values presented in this figure are not necessarily representative of typical flow velocities in a TWR.

Since the coolant flow is non-uniform at any given time, an appropriate mechanism to control the flow must be developed. It is suggested that controllable orifices be built at the base of the core (bottom X-Z plane in Figure 5.2). Detectors may be placed at the bottom of the core to monitor the local flux level (equivalent power level) and hence assist the reactor operator in controlling the coolant flow through that location. Temperatures measured at the exit of each zone may also be used to control the flow rate. The use of such controllable orifices at the inlet then allows the operator to monitor and control the flow through any given location in the core. Mechanical details of such controllable orifices in a TWR are not discussed in this thesis, and are a subject of further research.

Chapter 6

Summary, Conclusions and Future Work

6.1 Summary and conclusions

A 3-D box-shaped reactor with two-zone enrichment strategy is designed to study the space and time evolution of flux profile in a traveling wave reactor. The existence of a self-sustaining Nuclear Burning Wave (NBW) is shown using simulations carried out using MCNPX v27c. The flux profile is observed to propagate from enriched zone of the core to the non-enriched zone at a slightly faster rate during the early life of the core. It is concluded that an appropriate initial loading of fissile and fertile materials could sustain criticality over a long period, thus allowing for the core to operate under one-batch fuel cycle with no outage for refueling. Power densities are found to vary locally in the reactor core over time. This is mainly attributed to the space and time-evolving flux shape. Inventories for primary fertile and fissile materials are shown. The gradual decrease in fertile inventory (^{238}U) and simultaneous buildup of fissile inventory (^{239}Pu) over time is shown. This facilitates the breed-and-burn cycle. Simplified thermal-hydraulics analysis is carried out to calculate the core-averaged coolant flow rate. A time-dependent algorithm for heat removal based on flux profile is suggested and a sample calculation is presented to illustrate the proposed design.

6.2 Future work and recommendations

- The use of a right circular cylinder in place of a rectangular parallelepiped as a core minimizes fast leakage and is better suited for commercial design. A decrease in leakage will also help in reducing the initial enrichment levels compared to the current design.

- A homogeneous core is used in this study for neutronics calculations. For more accurate simulation of core physics, a heterogeneous core should be used. For example, distinct structures like fuel pins and triangular coolant channels should be modeled.
- Inventory of other minor actinides like americium, curium, berkelium, californium etc. must be kept and analyzed to ascertain a smaller waste stream compared to a thermal reactor.
- A smaller core is considered in this study. This, in turn, warranted a larger fuel volume fraction and a higher enrichment. To model a more realistic scenario, the size of the reactor should be increased and the enrichment level should be decreased. With sufficiently large size, the enrichment level could probably be brought down below 20% in ^{235}U.
- The possibility of coolant flow in the direction perpendicular to the Y-Z plane in Figure 5.2 (which is also the direction of wave propagation) may be explored. This will allow for an uniform coolant flow through the core, and will avoid complications associated with flux-profile-adjusted heat removal mechanism.

References

1. A. E. Walter, A. B. Reynolds, Fast Breeder Reactors, p. 9, p. 11, p. 436-450, 1981

2. M. B. Chadwick, P. Obložinský, M. Herman, N. M. Greene, R. D. McKnight, D. L. Smith, P. G. Young, R. E. MacFarlane, G. M. Hale, S. C. Frankle, A. C. Kahler, T. Kawano, R. C. Little, D. G. Madland, P. Moller, R. D. Mosteller, P. R. Page, P. Talou, H. Trellue, M. C. White, W. B. Wilson, R. Arcilla, C.L. Dunford, S. F. Mughabghab, B. Pritychenko, D. Rochman, A. A. Sonzogni, C. R. Lubitz, T. H. Trumbull, J. P. Weinman, D. A. Brown, D. E. Cullen, D. P. Heinrichs, D. P. McNabb, H. Derrien, M. E. Dunn, N. M. Larson, L.C. Leal, A.D. Carlson, R. C. Block, J. B. Briggs, E. T. Cheng, H. C. Huria, M. L. Zerkle, K. S. Kozier, A. Courcelle, V. Pronyaev, S. C. van der Marck, ENDF/B-VII.0: Next Generation Evaluated Nuclear Data Library for Nuclear Science and Technology, Nuclear Data Sheets, Vol. 107, I. 12, p. 2931-3060, December 2006

3. ENDF/B-VII Incident-Neutron Data, T2 Group at Los Alamos National Laboratory, Archived 15 July 2007, <http://t2.lanl.gov/data/n7-pdf/pu/239.pdf>

4. T. Ellis, R. Petroski, Traveling-Wave Reactors: A Truly Sustainable and Full-Scale Resource for Global Energy Needs, Proceedings of International Congress on Advances in Nuclear Power Plants 2010, June 13-17, 2010.

5. S. M. Feinberg, "Discussion Comment," *Rec. of Proc. Session B-10*, ICPUAE, United Nations, Geneva, Switzerland, 1958

6. L. Feoktistov, "Neutron-Fission Wave," *Dokl. Akad. Nauk*, SSSR, 309, No. 4, p. 864-867, 1989

7. V. D. Rusov, E. P. Linnik, V. A. Tarasov, T. N. Zelentsova, I. V. Sharph, V. N. Vaschenko, S. I. Kosenko, M. E. Beglaryan, S. A. Chernezhenko, P. A. Molchinikolov, S. I. Saulenko, O. A.

Byegunova, Traveling Wave Reactor and Condition of Existence of Nuclear Burning Soliton-Like Wave in Neutron-Multiplying Media, *Energies* 4(9), p. 1337-1361, 2011

8. X. N. Chen, W. Maschek, Nuclear Solitary Waves, PAMM, 8, p. 10489–10490, 2008

9. E. Teller, M. Ishikawa, L. Wood, "Completely Automated Nuclear Power Reactors for Long-Term Operation" *Proceedings of the Frontiers in Physics Symposium*, American Physical Society and the American Association of Physics Teachers Texas Meeting, Lubbock, TX, 1995

10. H. Sekimoto, K. Ryu, Y. Yoshimura, CANDLE: The New Burnup Strategy, Nuclear Science and Engineering; Vol. 139, I. 3, p. 306-317, Nov 2001

11. H. Sekimoto, S. Miyashita, Startup of "Candle" Burn-up in Fast Reactor From Enriched Uranium Core, Energy Conversion and Management, Vol. 47, I. 17, p. 2772-2780, October 2006.

12. S. P. Fomin, O. S. Fomin, Y. P.Mel'nik, V. V. Pilipenko, N. F. Shul'ga, Nuclear Burning Wave in Fast Reactor with Mixed Th-U fuel, Progress in Nuclear Energy, Vol. 53, I. 7, p. 800-805, September 2011

13. Y. I. Chang, P. L. Pinto, M. Konomura, Small Modular Fast Reactor Design Description, Argonne National Laboratory, ANL-SMFR-1, July 2005

14. R. N. Hill, Fast Reactor Physics and Core Design, NRC Topical Seminar on Sodium Fast Reactors, Two White Flint, Rockville, MD, May 2007

15. D. B. Pelowitz (editor), MCNPX User's Manual, LA-CP-07-1473, Los Alamos National Laboratory, 2008

16. L. Leibowitz and R. A. Blomquist, "Thermal Conductivity and Thermal Expansion of Stainless Steels D9 and HT9, "International Journal of Thermo-Physics, Vol. 9, No. 5, p. 873-883, September, 1988

17. T. Allen, J. Busby, R. Klueh, S. Maloy, M. Toloczko, Cladding and Duct Materials for Advanced Nuclear Recycle Reactors, Journal of the Minerals, Metals and Materials Society, Vol. 60, Number 1, p. 15-23, Jan 2008

18. T. H. Fanning, Sodium as a Fast Reactor, Topical Seminar Series on Sodium Fast Reactors, Two White Flint, Rockville, MD, May 2007

19. H. van Dam, Self-stabilizing criticality waves, Annals of Nuclear Energy, Vol. 27, p. 1505-1521, March 2000

20. H. Ninokata, E. Merzari, A. Khakim, Analysis of Low Reynolds Number Turbulent Flow Phenomena in Nuclear Fuel Pin Subassemblies of Tight Lattice Configuration, Nuclear Engineering and Design, Volume 239, Issue 5, Pages 855-866, May 2009

21. MCNPX home-page, Los Alamos National Laboratory, July 26, 2011, <http://mcnpx.lanl.gov/>

22. G. W. McKinney, M. R. James, "MCNPX 2.7.X - New Features Being Developed," LA-UR-09-6788, IEEE/NSS Conference, Orlando, FL, October 25-31, 2009

23. M. L. Fensin, J. S. Hendricks, S. Anghaie, "The Enhancements and Testing For the MCNPX 2.6.0 Depletion Capability," Journal of Nuclear Technology, 170, p. 68-79, April 2010

Appendix A

MCNPX Format for Input and Tally

MCNPX is a general purpose Monte Carlo radiation transport code used for modeling the interaction of radiation with matter. It stands for Monte Carlo N-Particle eXtended. It tracks nearly all particles over broad energy spectrum. It is written in Fortran 90 and runs on PC Windows, Linux, and UNIX platforms, and is fully parallel (PVM and MPI) [21]. It is fully three-dimensional and time dependent. It possesses powerful geometrical modeling capabilities, interactive graphics and could tally various variables of interest like particle current through a surface, particle flux in a cell, collision heat deposition in a cell, fission heat deposition in a cell etc. The particles could be alpha particle, neutron, proton, electron, photons etc [22]. It uses continuous energy cross-section data. The user has the option to choose from a variety of standard, tabulated cross-section data libraries.

An MCNPX input deck has three main sections: cell cards, surface cards and data cards. A single line card, known as title card, precedes the cell card section. A 'card' refers to a single line of input of up to 80 characters. A single section may contain one or more cards. Cell cards are used to define the location and shape of a physical region along with any material it may contain. Its specific format is:

a b c geom params

where, *a* is cell number starting in columns 1-5, *b* is material number (0 if cell is void), *c* is material density (either mass density or number density), *geom* is a list of all signed surface numbers that enclose the cell and *params* is optional specifications for cell parameters. The second section (surface cards) describes the surfaces that make up a physical region. Its specific format is:

d e params

where, *d* is the surface number starting in columns 1-5, *e* is surface designator (plane, sphere, parallelepiped etc.) and *params* is dimensions that describe the surface (length, radius etc., in cm). The final section is for the data cards. Data cards are used to specify if the problem is a source problem or a criticality problem. For criticality problems, *kcode* is used in the data card while *ksrc* is used as an identifier in the data card for source problems. The study in this thesis uses *kcode* for criticality calculations to determine the multiplication factors at various stages of reactor operation. The *kcode* has the following format:

kcode nsrck rkk ikz kct

where, *kcode* is used to identify criticality calculation, *nsrck* is the number of neutrons per cycle, *rkk* is initial guess for k_{eff}, ikz is the number of cycles skipped before collection of data and *kct* is total number of cycles to be run. Additionally, material cards must be provided following data cards for a complete MCNPX input. Its specific format is:

mn zaid1 fraction1 ….

where, *mn* is material card name (*m*) followed by material number (*n*), *zaid* is atomic number followed by atomic mass of the isotope in the form (*ZZZAAA*) and *fraction* is either nuclide fraction (positive) or weight fraction (negative). A given material may contain more than one isotope.

Variables of interest in MCNPX are stored in tallies. Tallies in MCNPX are identified by tally type and particle type. Tallies are numbered 1 through 8, with increments of 10 referring to the same tally type. Each tally is associated with an individual particle. For instance, when tally 4 (cell flux per source particle) is to be calculated, it has to be linked with a particular particle. In this study, flux of neutrons is the desired variable of interest. For a given region, it is tallied as follows:

F4: n M

Where, *F4: n* refers to the neutron flux per source particle in a prescribed volume (cell) identified by the number *M* (note that *M* corresponds to the cell number). The above could be equivalently represented as *F14: n M*.

The steady state (k) calculations are immediately followed by burn calculations in MCNPX. CINDER90 is incorporated into MCNPX which does burn-up calculations so there is no necessity for link-up program like MonteBurns. This automated process eliminates the need of a new input deck after each burn-up step. MCNPX performs a predictor-corrector calculation for each burn step. For the first half of a given burn step, it performs a predictor calculation for the flux profile, and then carries out burn-up calculations at half time step using the available flux profile from the predictor calculation. Then it updates the isotopic cross sections and performs a corrector calculation to generate the actual flux profile [23] at the end of each prescribed burn step.

Appendix B

MCNPX Input File

The following MCNPX input is used to model and analyze the Traveling Wave Reactor in this study.

```
Homogeneous box reactor
95 199 -14.29238 -121 -2     imp:n=1 vol=16200
96 199 -14.29238 -121 +2 -3  imp:n=1 vol=16200
97 199 -14.29238 -121 +3 -4  imp:n=1 vol=16200
98 199 -14.29238 -121 +4 -5  imp:n=1 vol=16200
99 199 -14.29238 -121 +5 -6  imp:n=1 vol=16200
100 200 -14.29238 -121 6 -7   imp:n=1 vol=16200
101 200 -14.29238 -121 7 -8   imp:n=1 vol=16200
102 200 -14.29238 -121 8 -9   imp:n=1 vol=16200
103 200 -14.29238 -121 9 -10  imp:n=1 vol=16200
104 200 -14.29238 -121 10 -11 imp:n=1 vol=16200
105 205 -14.29238 -121 11 -12 imp:n=1 vol=16200
106 205 -14.29238 -121 12 -13 imp:n=1 vol=16200
107 205 -14.29238 -121 13 -14 imp:n=1 vol=16200
108 205 -14.29238 -121 14 -15 imp:n=1 vol=16200
109 205 -14.29238 -121 15 -16 imp:n=1 vol=16200
110 206 -14.29238 -121 16 -17 imp:n=1 vol=16200
111 206 -14.29238 -121 17 -18 imp:n=1 vol=16200
112 206 -14.29238 -121 18 -19 imp:n=1 vol=16200
113 206 -14.29238 -121 19 -20 imp:n=1 vol=16200
114 206 -14.29238 -121 20 -21 imp:n=1 vol=16200
115 207 -14.29238 -121 21 -22 imp:n=1 vol=16200
116 207 -14.29238 -121 22 -23 imp:n=1 vol=16200
117 207 -14.29238 -121 23 -24 imp:n=1 vol=16200
118 207 -14.29238 -121 24 -25 imp:n=1 vol=16200
119 207 -14.29238 -121 25 -26 imp:n=1 vol=16200
120 208 -14.29238 -121 26 -27 imp:n=1 vol=16200
121 208 -14.29238 -121 27 -28 imp:n=1 vol=16200
122 208 -14.29238 -121 28 -29 imp:n=1 vol=16200
123 208 -14.29238 -121 29 -30 imp:n=1 vol=16200
124 208 -14.29238 -121 30 -31 imp:n=1 vol=16200
125 209 -14.29238 -121 31 -32 imp:n=1 vol=16200
126 209 -14.29238 -121 32 -33 imp:n=1 vol=16200
127 209 -14.29238 -121 33 -34 imp:n=1 vol=16200
128 209 -14.29238 -121 34 -35 imp:n=1 vol=16200
129 209 -14.29238 -121 35 -36 imp:n=1 vol=16200
130 210 -14.29238 -121 36 -37 imp:n=1 vol=16200
131 210 -14.29238 -121 37 -38 imp:n=1 vol=16200
```

```
132 210 -14.29238 -121 38 -39 imp:n=1 vol=16200
133 210 -14.29238 -121 39 -40 imp:n=1 vol=16200
134 210 -14.29238 -121 40 -41 imp:n=1 vol=16200
135 211 -14.29238 -121 41 -42 imp:n=1 vol=16200
136 211 -14.29238 -121 42 -43 imp:n=1 vol=16200
137 211 -14.29238 -121 43 -44 imp:n=1 vol=16200
138 211 -14.29238 -121 44 -45 imp:n=1 vol=16200
139 211 -14.29238 -121 45 -46 imp:n=1 vol=16200
140 212 -14.29238 -121 46 -47 imp:n=1 vol=16200
141 212 -14.29238 -121 47 -48 imp:n=1 vol=16200
142 212 -14.29238 -121 48 -49 imp:n=1 vol=16200
143 212 -14.29238 -121 49 -50 imp:n=1 vol=16200
144 212 -14.29238 -121 50 -51 imp:n=1 vol=16200
145 213 -14.29238 -121 51 -52 imp:n=1 vol=16200
146 213 -14.29238 -121 52 -53 imp:n=1 vol=16200
147 213 -14.29238 -121 53 -54 imp:n=1 vol=16200
148 213 -14.29238 -121 54 -55 imp:n=1 vol=16200
149 213 -14.29238 -121 55 -56 imp:n=1 vol=16200
150 214 -14.29238 -121 56 -57 imp:n=1 vol=16200
151 214 -14.29238 -121 57 -58 imp:n=1 vol=16200
152 214 -14.29238 -121 58 -59 imp:n=1 vol=16200
153 214 -14.29238 -121 59 -60 imp:n=1 vol=16200
154 214 -14.29238 -121 60 -61 imp:n=1 vol=16200
155 215 -14.29238 -121 61 -62 imp:n=1 vol=16200
156 215 -14.29238 -121 62 -63 imp:n=1 vol=16200
157 215 -14.29238 -121 63 -64 imp:n=1 vol=16200
158 215 -14.29238 -121 64 -65 imp:n=1 vol=16200
159 215 -14.29238 -121 65 -66 imp:n=1 vol=16200
160 216 -14.29238 -121 66 -67 imp:n=1 vol=16200
161 216 -14.29238 -121 67 -68 imp:n=1 vol=16200
162 216 -14.29238 -121 68 -69 imp:n=1 vol=16200
163 216 -14.29238 -121 69 -70 imp:n=1 vol=16200
164 216 -14.29238 -121 70     imp:n=1 vol=16200
165 250 -6.3694   +121 -120   imp:n=1 vol=802000
166 0             +120        imp:n=0

c surface cards
120 rpp -10  150 0  110 0  110
121 rpp  0   140 10 100 10 100
2 px 2
3 px 4
4 px 6
5 px 8
6 px 10
7 px 12
8 px 14
9 px 16
10 px 18
11 px 20
12 px 22
13 px 24
14 px 26
15 px 28
16 px 30
17 px 32
18 px 34
```

19 px 36
20 px 38
21 px 40
22 px 42
23 px 44
24 px 46
25 px 48
26 px 50
27 px 52
28 px 54
29 px 56
30 px 58
31 px 60
32 px 62
33 px 64
34 px 66
35 px 68
36 px 70
37 px 72
38 px 74
39 px 76
40 px 78
41 px 80
42 px 82
43 px 84
44 px 86
45 px 88
46 px 90
47 px 92
48 px 94
49 px 96
50 px 98
51 px 100
52 px 102
53 px 104
54 px 106
55 px 108
56 px 110
57 px 112
58 px 114
59 px 116
60 px 118
61 px 120
62 px 122
63 px 124
64 px 126
65 px 128
66 px 130
67 px 132
68 px 134
69 px 136
70 px 138

c data cards
mode n
kcode 10000 1 30 145

```
ksrc  1 50 50 3 50 50 5 50 50 7 50 50 9 50 50
      11 50 50 13 50 50 15 50 50 17 50 50 19 50 50 21 50 50
      23 50 50 25 50 50 27 50 50 29 50 50 31 50 50 33 50 50
      35 50 50 37 50 50 39 50 50 41 50 50 43 50 50 45 50 50
      47 50 50 49 50 50 51 50 50 53 50 50 55 50 50 57 50 50
      59 50 50 61 50 50 63 50 50 65 50 50 67 50 50 69 50 50
      71 50 50 73 50 50 75 50 50 77 50 50 79 50 50 81 50 50
      83 50 50 85 50 50 87 50 50 89 50 50 91 50 50 93 50 50
      95 50 50 97 50 50 99 50 50 101 50 50 103 50 50
      105 50 50 107 50 50 109 50 50 111 50 50 113 50 50
      115 50 50  117 50 50  119 50 50 121 50 50
      123 50 50  125 50 50 127 50 50  129 50 50
      131 50 50  133 50 50  135 50 50  137 50 50  139 50 50
prdmp j j 1 j j
BURN
      TIME =   30 1200 14r   $ days
      PFRAC = 1  1    14r    $ Fraction
      POWER = 350            $ Power level MW
      MAT=199 200 205 206 207
         208 209 210 211
         212 213 214 215
         216
      MATVOL= 81000 13r
      BOPT=   1 4 1
c compositions
c 33 % in U-235 and natural uranium
m199 40091 0.185617544
     92235 0.211294689
     92238 0.428992248
     11023 0.035101832
     26056 0.115903852
     24052 0.017666491
     28059 0.000808517
     74184 0.000200712
     42096 0.000825497
     25055 0.000965241
     14028 0.000824352
     23051 0.000452585
     6012 0.001346441
m200 40091 0.185617544
     92235 0.211294689
     92238 0.428992248
     11023 0.035101832
     26056 0.115903852
     24052 0.017666491
     28059 0.000808517
     74184 0.000200712
     42096 0.000825497
     25055 0.000965241
     14028 0.000824352
     23051 0.000452585
     6012 0.001346441
m205 40091 0.185617544
     92235 0.211294689
     92238 0.428992248
     11023 0.035101832
```

26056 0.115903852
24052 0.017666491
28059 0.000808517
74184 0.000200712
42096 0.000825497
25055 0.000965241
14028 0.000824352
23051 0.000452585
6012 0.001346441
c
m206 40091 0.185617544
92235 0.004482009
92238 0.635804929
11023 0.035101832
26056 0.115903852
24052 0.017666491
28059 0.000808517
74184 0.000200712
42096 0.000825497
25055 0.000965241
14028 0.000824352
23051 0.000452585
6012 0.001346441
m207 40091 0.185617544
92235 0.004482009
92238 0.635804929
11023 0.035101832
26056 0.115903852
24052 0.017666491
28059 0.000808517
74184 0.000200712
42096 0.000825497
25055 0.000965241
14028 0.000824352
23051 0.000452585
6012 0.001346441
m208 40091 0.185617544
92235 0.004482009
92238 0.635804929
11023 0.035101832
26056 0.115903852
24052 0.017666491
28059 0.000808517
74184 0.000200712
42096 0.000825497
25055 0.000965241
14028 0.000824352
23051 0.000452585
6012 0.001346441
m209 40091 0.185617544
92235 0.004482009
92238 0.635804929
11023 0.035101832
26056 0.115903852
24052 0.017666491
28059 0.000808517

74184 0.000200712
42096 0.000825497
25055 0.000965241
14028 0.000824352
23051 0.000452585
6012 0.001346441
m210 40091 0.185617544
92235 0.004482009
92238 0.635804929
11023 0.035101832
26056 0.115903852
24052 0.017666491
28059 0.000808517
74184 0.000200712
42096 0.000825497
25055 0.000965241
14028 0.000824352
23051 0.000452585
6012 0.001346441
m211 40091 0.185617544
92235 0.004482009
92238 0.635804929
11023 0.035101832
26056 0.115903852
24052 0.017666491
28059 0.000808517
74184 0.000200712
42096 0.000825497
25055 0.000965241
14028 0.000824352
23051 0.000452585
6012 0.001346441
m212 40091 0.185617544
92235 0.004482009
92238 0.635804929
11023 0.035101832
26056 0.115903852
24052 0.017666491
28059 0.000808517
74184 0.000200712
42096 0.000825497
25055 0.000965241
14028 0.000824352
23051 0.000452585
6012 0.001346441
m213 40091 0.185617544
92235 0.004482009
92238 0.635804929
11023 0.035101832
26056 0.115903852
24052 0.017666491
28059 0.000808517
74184 0.000200712
42096 0.000825497
25055 0.000965241
14028 0.000824352

23051 0.000452585
6012 0.001346441
m214 40091 0.185617544
92235 0.004482009
92238 0.635804929
11023 0.035101832
26056 0.115903852
24052 0.017666491
28059 0.000808517
74184 0.000200712
42096 0.000825497
25055 0.000965241
14028 0.000824352
23051 0.000452585
6012 0.001346441
m215 40091 0.185617544
92235 0.004482009
92238 0.635804929
11023 0.035101832
26056 0.115903852
24052 0.017666491
28059 0.000808517
74184 0.000200712
42096 0.000825497
25055 0.000965241
14028 0.000824352
23051 0.000452585
6012 0.001346441
m216 40091 0.185617544
92235 0.004482009
92238 0.635804929
11023 0.035101832
26056 0.115903852
24052 0.017666491
28059 0.000808517
74184 0.000200712
42096 0.000825497
25055 0.000965241
14028 0.000824352
23051 0.000452585
6012 0.001346441
m250 26056 0.77775928
24052 0.118548931
28059 0.005425457
74184 0.001346853
42096 0.005539399
25055 0.006477137
14028 0.005531716
23051 0.003037021
6012 0.009035136
11023 0.067299071
c
f4:n 95 96 97 98 99 100 101 102 103 104 105 106 107 108 109
110 111 112 113
114 115 116 117 118 119 120 121 122 123 124 125 126 127
128 129 130 131 132 133 134 135 136 137 138 139 140 141

142 143 144 145 146 147 148 149 150 151 152 153 154 155
156 157 158 159 160 161 162 163 164
e4 0.0000001 8LOG 100
f6:n 95 96 97 98 99 100 101 102 103 104 105 106 107 108 109
110 111 112 113
114 115 116 117 118 119 120 121 122 123 124 125 126 127
128 129 130 131 132 133 134 135 136 137 138 139 140 141
142 143 144 145 146 147 148 149 150 151 152 153 154 155
156 157 158 159 160 161 162 163 164
f7:n 95 96 97 98 99 100 101 102 103 104 105 106 107 108 109
110 111 112 113
114 115 116 117 118 119 120 121 122 123 124 125 126 127
128 129 130 131 132 133 134 135 136 137 138 139 140 141
142 143 144 145 146 147 148 149 150 151 152 153 154 155
156 157 158 159 160 161 162 163 164